A Simple Dynamical Model with Features of Convective Momentum Transport

ANDREW J. MAJDA AND SAMUEL N. STECHMANN

Department of Mathematics, and Center for Atmosphere–Ocean Science, Courant Institute, New York University, New York, New York

(Manuscript received 3 April 2008, in final form 16 July 2008)

ABSTRACT

Convective momentum transport (CMT) plays a central role in interactions across multiple space and time scales. However, because of the multiscale nature of CMT, quantifying and parameterizing its effects is often a challenge. Here a simple dynamic model with features of CMT is systematically derived and studied. The model includes interactions between a large-scale zonal mean flow and convectively coupled gravity waves, and convection is parameterized using a multicloud model.

The moist convective wave–mean flow interactions shown here have several interesting features that distinguish them from other classical wave–mean flow settings. First an intraseasonal oscillation of the mean flow and convectively coupled waves (CCWs) is described. The mean flow oscillates due to both upscale and downscale CMT, and the CCWs weaken, change their propagation direction, and strengthen as the mean flow oscillates. The basic mechanisms of this oscillation are corroborated by linear stability theory with different mean flow background states.

Another case is set up to imitate the westerly wind burst phase of the Madden–Julian oscillation (MJO) in the simplified dynamic model. In this case, CMT first accelerates the zonal jet with the strongest westerly wind aloft, and then there is deceleration of the winds due to CMT; this occurs on an intraseasonal time scale and is in qualitative agreement with actual observations of the MJO. Also, in this case, a multiscale envelope of convection propagates westward with smaller-scale convection propagating eastward within the envelope. The simplified dynamic model is able to produce this variety of behavior even though it has only a single horizontal direction and no Coriolis effect.

1. Introduction

Convective momentum transport (CMT) is the process of conversion of (moist) convective available potential energy to horizontal kinetic energy in the flow field. The significance of CMT for the organization of cumulus convection on mesoscales is well known (Moncrieff 1981; LeMone 1983; LeMone et al. 1984, and references therein), and many important studies on the parameterization of CMT have been conducted. For instance, Wu and Yanai (1994) developed a parameterization of CMT based on a cumulus mass flux spectrum (Wu et al. 2007). Wu and Moncrieff (1996) showed in a cloud-resolving model (CRM) simulation that the generation of kinetic energy by CMT-generated shear is comparable to buoyancy generation and dominates the total buoyancy; thus, they argued for the need to represent CMT in convective parameterizations.

Besides these results on CMT due to mesoscale convection, CMT is also thought to play a central role at both the synoptic and planetary scales in multiscale interactions in the tropical atmosphere. Below are several examples that illustrate the importance of CMT through this range of larger scales.

It is well known from observations that the zonal winds in the tropics oscillate on intraseasonal time scales because of the Madden–Julian oscillation (MJO; Madden and Julian 1972, 1994). Many details of the structure of the MJO have been examined in statistical composites of reanalysis data (Hendon and Salby 1994; Kiladis et al. 2005) and in observations of two individual MJO events that occurred during the Tropical Ocean Global Atmosphere Coupled Ocean–Atmosphere Response Experiment (TOGA COARE; Lin and Johnson 1996; Yanai et al. 2000; Houze et al. 2000). Yanai et al. (2000) showed the dominant effect in the MJO of conversion of available potential energy, generated by convective

Corresponding author address: Samuel N. Stechmann, Courant Institute, New York University, 251 Mercer Street, New York, NY 10012.
E-mail: stechman@cims.nyu.edu

DOI: 10.1175/2008JAS2805.1

heating, to kinetic energy. Tung and Yanai (2002a,b) showed that on average CMT is downscale (damping on the large scales) but also that the fluctuations about the mean are very large, with intense bursts of upscale transport (amplification on the large scales). In the westerly wind burst regime of the MJO, they found first upscale and then downscale CMT. A well-known theoretical model for the MJO that roughly agrees with observations is a first baroclinic Kelvin–Rossby wave (Houze et al. 2000), but this paradigm does not account for important features of the observational record such as the midlevel westerly jet of the westerly wind burst and the horizontal quadrupole vortices. These latter features have been captured in more refined diagnostic models of the MJO that suggest they are a result of CMT from synoptic-scale waves (Majda and Biello 2004, hereafter MB04; Biello and Majda 2005, hereafter BM05).

CMT on other scales has been posited to play a key role in the ''MJO-like'' structures in ''superparameterization'' computer simulations (Grabowski 2002, 2003, 2004; Moncrieff 2004). Further evidence of the dynamic role of CMT in those MJO-like structures is that the MJO-like wave develops when the small-scale 2D models are oriented in the east–west direction, favoring zonal CMT; but the MJO-like wave does not develop when the small-scale 2D models are oriented in the north–south direction (Grabowski 2002).

CMT also appears to be important in superclusters and CRM simulations of superclusters. The approximate self-similarity of tropical convection—from mesoscale cloud clusters to synoptic-scale superclusters to the planetary-scale MJO—has been documented in observations (Mapes et al. 2006) and a framework for this self-similarity has been developed, with CMT playing a central role in the multiscale interactions (Majda 2007b). In CRM simulations of superclusters on large one-dimensional horizontal periodic domains on the order of 10 000 km, the importance of CMT varies because different studies have used large-scale momentum damping of different strengths. For instance, CMT plays an active role in the simulations of Grabowski and Moncrieff (2001), but CMT is inactive in the simulations of Tulich et al. (2007), which have much stronger momentum damping. In addition, the pioneering CRM studies of Held et al. (1993) on a smaller mesoscale periodic domain of 640 km displayed an oscillation of the zonal wind that was called ''QBO-like'' because it resembled the quasi-biennial oscillation (QBO) of the tropical stratosphere. This QBO-like oscillation was shut down when the domain-mean momentum was damped. In their discussion section, it was asked whether the oscillation in the troposphere is due to interactions with the stratosphere or due to CMT. The other results in this paragraph suggest that CMT might play a central role.

A common theme from the CMT examples above is that upscale transports from CMT can alter the large-scale mean flow on both synoptic and planetary scales. Much has been learned about this process through models that diagnose the waves that generate the CMT (Moncrieff 1992, 2004; MB04; BM05). The goal here is to develop a simple dynamical model that demonstrates the nonlinear interaction between a large-scale mean flow and convectively coupled waves (CCWs) with relevance for the synoptic and planetary scales. The important features to capture in such a dynamical model are that the mean flow can respond to the CCWs through upscale and downscale CMT, and, simultaneously, that the nature of the mean flow determines the character of the convection and waves; thus, there are two-way interactions that need to be modeled.

The model developed here takes into account important characteristics of CCWs from the observational record. Convectively coupled Kelvin waves and 2-day waves are a prominent feature of the observational record on equatorial synoptic scales on the order of 1500 to 6000 km (Wheeler and Kiladis 1999; Yang et al. 2007a,b,c); a prominent observed feature of these CCWs is a vertical tilt, which means that they can transport momentum to larger scales (see section 2e below for an elementary explicit demonstration). Here we utilize a recently developed multicloud model for CCWs with crude vertical resolution (Khouider and Majda 2006c, hereafter KM06c, 2007, 2008b, hereafter KM08b) to provide a base dynamical model for the CCWs. This model includes the effect of three cloud types—deep convective, stratiform, and congestus—and, like the observations, its CCWs have vertical tilts, which are crucial for CMT. The complete dynamical model involves a one-dimensional horizontal periodic domain with a large-scale, spatially independent mean flow. The mean flow responds to the waves through CMT and upscale moisture and temperature fluxes, and, in turn, it alters the CCWs primarily through advection by the large-scale winds and mean moist thermodynamic state. Although it is well known that the properties of mesoscale convective systems are determined by the environmental shear and thermodynamic conditions (Barnes and Sieckman 1984; Dudhia et al. 1987; Nicholls et al. 1988; LeMone et al. 1998; Lucas et al. 2000), it is less well understood how CCWs can have different properties depending on the large-scale environment (Wheeler and Kiladis 1999; Roundy and Frank 2004; Yang et al. 2007a,b,c). This is an important feature that the dynamical model developed here attempts to capture in addition to CMT. As shown below, this

model has important features that distinguish it from models of classical wave–mean flow interactions [such as the QBO (Baldwin et al. 2001) and midlatitude baroclinic instability (Vallis 2006)].

The rest of the paper is organized as follows: The dynamic model is systematically derived and described in section 2. The simplest scenario with a regular intraseasonal oscillation of the mean flow is described in section 3, and cases with irregular oscillations and a climate base state are described in section 4. A discussion and conclusions follow in sections 5 and 6.

2. The dynamic model

The model used here consists of two parts. The first part describes the mean variables and the second part describes the waves. Conceptually, the model then takes the form (using the zonal velocity as an example)

$$\frac{\partial \bar{U}}{\partial T} + \frac{\partial}{\partial z}\langle \overline{w'u'} \rangle = 0 \tag{1}$$

$$\frac{\partial u'}{\partial t} + \bar{U}\frac{\partial u'}{\partial x} + w'\frac{\partial \bar{U}}{\partial z} + \frac{\partial p'}{\partial x} = S'_{u,1}, \tag{2}$$

where the notation is standard and described below, with u' describing the smaller-scale fluctuations and $\bar{U}$ the large-scale mean. Key interactions are (i) eddy flux convergence of wave momentum $\partial_z\langle \overline{w'u'} \rangle$ feeding the mean flow $\bar{U}$ and (ii) advection of the waves u' by the mean flow $\bar{U}$. The time scale $T = \epsilon^2 t$ for the changes of the zonal mean flows in (1) is longer than that for the waves and is explained below. At this stage of the discussion, $S'_{u,1}$ is a source of momentum for the smaller scales, which will be described in more detail below.

This section is organized as follows: The starting point for the model is the multicloud model of KM08b with advection, which is described in section 2a. The equations for the mean and wave variables are obtained from this model in sections 2b and 2c, respectively. In section 2d, a systematic derivation of these wave-mean equations is presented using multiscale asymptotics. A discussion of CMT and wave tilts is given in section 2e, and the numerical methods for the wave-mean equations are described in section 2f. Here only central or illustrative components of the model are described to streamline the presentation; details and complex formulas are relegated to appendices.

a. Multicloud model with advection

The starting point for the model is the multicloud model of KM08b with advection terms added. The multicloud model is so named because it provides a simple dynamical framework that parameterizes the effect of three cloud types—deep convective, stratiform, and congestus clouds—that are prominent in the observational record (Johnson et al. 1999). The original form of this model was described by KM06c, and the detailed structure of the CCWs in the model, including fidelity with the observations, has been documented extensively through linear theory (KM06c; Khouider and Majda 2006b, 2008a; KM08b) and in nonlinear simulations (Khouider and Majda 2006a, 2007; KM08b). A key feature of the multicloud models in agreement with observations is the westward (eastward) tilt with height in an eastward- (westward-) propagating CCW, which allows for nonzero CMT onto the larger scales. This is a crucial feature for the dynamical models developed here.

In the multicloud model, the dynamical variables have a crude vertical structure that includes two vertical baroclinic modes:

$$u(x,z,t) = u_1(x,t)\sqrt{2}\cos(z) + u_2(x,t)\sqrt{2}\cos(2z) \tag{3}$$

$$\theta(x,z,t) = z + \theta_1(x,t)\sqrt{2}\sin(z) + \theta_2(x,t)2\sqrt{2}\sin(2z), \quad \text{for} \quad 0 \le z \le \pi, \tag{4}$$

where z has been nondimensionalized so that $z = 0$ at the surface and $z = \pi$ at the tropopause. Notice that the total potential temperature also includes a linear background stratification (which has been nondimensionalized). The setup used here is two-dimensional (x–z) above the equator, so rotational effects of the Coriolis terms are ignored. The variables are nondimensionalized using the standard equatorial reference scales listed in Table 1 (see also, e.g., Majda 2007b). Thus, the basic spatial scale in the dynamic model is the equatorial synoptic scale on the order of 1500 km.

Here the multicloud model of KM08b is used with nonlinear advection terms added as done by Stechmann et al. (2008). The full set of equations is shown in appendix A. To illustrate the main features of the multicloud model with advection, consider the equations for u_2 and θ_2, the second baroclinic velocity and potential temperature:

$$\frac{\partial u_2}{\partial t} - \frac{\partial \theta_2}{\partial x} = -\frac{1}{\tau_u}u_2 - 2\sqrt{2}\,\bar{U}_3\frac{\partial u_1}{\partial x} \tag{5}$$

$$= S_u + A_u \tag{6}$$

$$\frac{\partial \theta_2}{\partial t} - \frac{1}{4}\frac{\partial u_2}{\partial x} = H_c - H_s - R_2 - \frac{1}{2\sqrt{2}}\left[(u_1 - \bar{U}_3)\frac{\partial \theta_1}{\partial x} - (\theta_1 - 9\bar{\Theta}_3)\frac{\partial u_1}{\partial x} + 8\bar{\Theta}_4\frac{\partial u_2}{\partial x}\right] \tag{7}$$

$$= S_\theta + A_\theta, \tag{8}$$

TABLE 1. Physical parameters and reference scales.

Parameter	Derivation	Value	Description
β		2.3×10^{-11} m^{-1} s^{-1}	Variation of Coriolis parameter with latitude
θ_{ref}		300 K	Reference potential temperature
g		9.8 m s^{-2}	Gravitational acceleration
H		16 km	Tropopause height
N^2	$(g/\theta_{\text{ref}})d\theta_{\text{bg}}/dz$	10^{-4} s^{-2}	Buoyancy frequency squared
c	NH/π	50 m s^{-1}	Velocity scale
L	$\sqrt{c/\beta}$	1500 km	Equatorial length scale
T_E	L/c	8 h	Equatorial time scale
$\bar{\alpha}$	$HN^2\theta_{\text{ref}}/(\pi g)$	15 K	Potential temperature scale
	H/π	5 km	Vertical length scale
	$H/(\pi T_E)$	0.2 m s^{-1}	Vertical velocity scale
	c^2	2500 m^2 s^{-2}	Pressure scale

where the nonlinear advection terms and source terms are denoted by A and S, respectively. The source terms H_c and H_s represent heating from congestus and stratiform clouds, and R_2 represents radiative cooling of the second baroclinic mode. In (7), the terms in brackets on the right-hand side are the projection of nonlinear advection terms $u\partial_x\theta + w\partial_z\theta$ onto the second baroclinic mode, and the linear advection term on the left-hand side is due to the background stratification. Advection terms involving the third and fourth baroclinic modes are shown for zonally averaged variables $\bar{U}_3, \bar{\Theta}_3$, and $\bar{\Theta}_4$. See appendix A and KM08b for more details of the multicloud model, and see Stechmann et al. (2008) for more details on the nonlinear advection terms.

The equations for the mean flow and the CCWs are derived below by essentially averaging the multicloud model with advection (although there are a few caveats). The variables are split into mean and fluctuating components by using a space–time average discussed below:

$$u_2(x,t) = \bar{U}_2(T) + u_2'(x,t), \tag{9}$$

with similar expressions for the other variables, and where $T = \epsilon^2 t$ is a slow (intraseasonal) time scale, as also explained below.

b. Equations for mean variables

To obtain equations for the mean variables, a space–time average is applied to the multicloud model with advection shown in (5)–(8) and in appendix A. The averaging involves a spatial average (denoted $\bar{f}$) over the periodic domain and a time average (denoted $\langle f \rangle$) that is explained below. The space–time average of, for instance, u_2 will be denoted by $\bar{U}_2$. Using $\bar{U}_2$ and $\bar{\Theta}_2$ as examples, Eqs. (5)– (8) are averaged to give

$$\frac{\partial \bar{U}_2}{\partial T} = \langle \overline{A_u} \rangle \quad \text{and} \tag{10}$$

$$\frac{\partial \bar{\Theta}_2}{\partial T} = \langle \overline{S_\theta} \rangle + \langle \overline{A_\theta} \rangle. \tag{11}$$

As mentioned above, there is a caveat that makes these equations differ from a simple space–time average of (5)–(8): the large-scale average of the momentum source terms, $\langle \overline{S_u} \rangle = -\bar{U}_2/\tau_u$, is *not* included. The reason for this is that the momentum drag $-u_2/\tau_u$ is a parameterization of unresolved CMT, but the CMT affecting $\bar{U}_2$ is resolved by the eddy flux divergence $\langle \overline{A_u} \rangle$, so there is no need for a parameterization.

Another caveat is that mean variables are included for the third and fourth baroclinic modes ($\bar{U}_3, \bar{\Theta}_3$, and $\bar{\Theta}_4$), but the fluctuations of these modes (u_3', θ_3', and θ_4') will not be represented in the multicloud model for the CCWs. In fact, because the multicloud model includes wave momentum in only the first two baroclinic modes, it is only possible for the first four baroclinic modes to be affected by the advection terms $\langle \overline{A_u} \rangle$ and $\langle \overline{A_\theta} \rangle$.To illustrate the explicit form of the averaged advection terms, $\langle \overline{A_u} \rangle$ and $\langle \overline{A_\theta} \rangle$, consider the form of $\langle \overline{A_u} \rangle$ for $\bar{U}_j, j = 1,2,3$. The mean flow equations for the different baroclinic modes are

$$\frac{d\bar{U}_1}{dT} = -\frac{1}{\sqrt{2}} \left\langle \overline{u_2' \frac{\partial u_1'}{\partial x} - \frac{1}{2} u_1' \frac{\partial u_2'}{\partial x}} \right\rangle, \tag{12}$$

$$\frac{d\bar{U}_2}{dT} = 0, \quad \text{and} \tag{13}$$

$$\frac{d\bar{U}_3}{dT} = -\frac{3}{\sqrt{2}} \left\langle \overline{-u_2' \frac{\partial u_1'}{\partial x} - \frac{1}{2} u_1' \frac{\partial u_2'}{\partial x}} \right\rangle. \tag{14}$$

The mean thermodynamic variables satisfy similar equations that are obtained by space–time averaging the multicloud model equations shown in appendix A.

Although one might also expect $\bar{U}_4$ to be needed here, it turns out that waves with only first and second baroclinic components can excite $\bar{\Theta}_4$ but not $\bar{U}_4$. This is because the incompressibility equation leads to $w_2(x, t)\sin(2z) = -\partial_x u_2(x, t)\sin(2z)/2$, from which it follows that $\overline{w_2' u_2'} = -\overline{u_2' \partial_x u_2'}/2 = 0$. On the other hand, $\bar{\Theta}_4$ is needed because $\overline{w_2' \theta_2'} \neq 0$.

c. Equations for convectively coupled waves

The equations for the synoptic-scale fluctuating CCWs are obtained by decomposing each variable into mean and fluctuation parts as, for instance, $u_2(x,t) = \bar{U}_2(T) + u_2'(x,t)$. The wave equations are then obtained by subtracting the mean equations [such as (13)] from the full equations [such as (5)]. For example, the equation for u_2' is

$$\frac{\partial u_2'}{\partial t} - \frac{\partial \theta_2'}{\partial x} = -\frac{1}{\tau_u} u_2' - 2\sqrt{2}\bar{U}_3 \frac{\partial u_1'}{\partial x}, \tag{15}$$

where the caveat regarding momentum damping was respected. Note that u_3, θ_3, and θ_4 have mean components but no wave components. Also note that $\bar{U}_4$ is not needed here for the reason given at the end of section 2b.

d. Asymptotic description of convectively coupled wave–mean flow interactions

The model described above includes two parts: a model for the mean variables, such as $\bar{U}_2$, and a model for the waves, such as u_2'. The main interactions between the waves and means occur through (i) eddy flux divergences feeding the mean variables and (ii) advection of the waves by the mean variables. This model can also be described in a framework of multiscale asymptotics (Majda and Klein 2003; Majda 2003, 2007b,a; A. Majda and Y. Xing 2009, hereafter MaXi). A partial description of the asymptotic model is given here for the zonal velocity u, and a full derivation is given in appendix B. These asymptotic equations serve as motivation for the form of the model in sections 2c and 2b. They also serve as a partial explanation for the evolution of the mean flow on intraseasonal time scales, which is described later in sections 3 and 4.

Assume the zonal velocity u consists of a mean flow $\bar{U}$ and waves u':

$$u = \bar{U}(z, \epsilon^2 t) + \epsilon u'(x, z, t, \epsilon^2 t) + O(\epsilon^2), \tag{16}$$

where $\epsilon \ll 1$ is a small parameter and x and t have been nondimensionalized by the reference values in Table 1. The parameter ϵ is essentially the Froude number as in Majda (2007b). Thus, the zonal mean flow can be large (up to 50 m s^{-1}), whereas the waves are weaker (on the order of 5 m s^{-1}). The mean flow $\bar{U}$ is a function of height z and a long time scale $\epsilon^2 t$, and it is a zonally averaged flow. The waves $\epsilon u'$ are also functions of the zonal coordinate x and the synoptic time scale t, and they are $O(\epsilon)$ in magnitude. Other variables (pressure p, potential temperature θ, etc.) are assumed to have similar expansions, and u is assumed to evolve as

$$\frac{\partial u}{\partial t} + u\frac{\partial u}{\partial x} + w\frac{\partial u}{\partial z} + \frac{\partial p}{\partial x} = S_u, \tag{17}$$

where S_u is a momentum source. With these assumptions, the equations for wave–mean flow interaction from (1) and (2) can be derived using multiscale asymptotics. The notation $f = \bar{f} + f'$ is a decomposition into zonal mean and fluctuation, and the angle brackets $\langle f \rangle$ denote an average over the synoptic time scale t. (The time average is described in a practical setting in section 2f and in a theoretical setting in appendix B.) The mean flow $\bar{U}$ evolves on an intraseasonal time scale $T = \epsilon^2 t$, and it is altered by eddy flux divergence of wave momentum, $\partial_z \langle \overline{w'u'} \rangle$. The waves u' evolve on the synoptic time scale t (and are modulated on the intraseasonal time scale $T = \epsilon^2 t$) and are advected by the large-scale mean flow $\bar{U}$. Thus, there are two-way feedbacks between the waves and the mean flow. See appendix B for details of the derivation and the equations for other variables. See MaXi for another example of squall line dynamics of multiscale asymptotics with a nonlow Froude number velocity contribution from $\bar{U}$.

Note that a choice of $\epsilon \approx 0.1$ implies that $T = \epsilon^2 t$ is an intraseasonal time variable. To see this, recall that t is nondimensionalized by the reference scale $T_E \approx 8$ h (see Table 1). Thus, t has magnitude $O(1)$ on the time scale $T_E \approx 8$ h, and it has magnitude $O(\epsilon^{-2})$ on the time scale $\epsilon^{-2} T_E \approx 30$ days. The variable $T = \epsilon^2 t$ then has magnitude $O(1)$ on the intraseasonal time scale $\epsilon^{-2} T_E \approx 30$ days, so it is an intraseasonal time variable. In addition, the choice $\epsilon \approx 0.1$ also implies low Froude number dynamics for the CCWs in the ansatz in (16), and this scaling is corroborated by numerical simulations in subsequent sections with the model (see Fig. 4).

e. Momentum transport and wave tilts

Earlier studies of CMT have emphasized the importance of wave tilts for upscale momentum transport (Moncrieff 1992; MB04; BM05). Because the multicloud model used here for the CCWs includes two baroclinic modes, the CCWs are tilted with height and can transport momentum upscale or downscale. Recall from earlier discussion that the CCWs in the multicloud model, like the observations, have a westward (eastward) tilt with height in an eastward- (westward)

propagating CCW (KM06c; Khouider and Majda 2006a, 2007, 2008a; KM08b).

A simple kinematic illustration of these effects can be made with a weak temperature gradient (WTG) model, which has been derived, for instance, in the multiscale balanced mesoscale equatorial synoptic dynamical (BMESD) model of Majda (2007b). This model applies to equatorial synoptic scales on the order of 1500 km. In this model, there is a balance ($w' = S'_\theta$) between the vertical velocity w' and the potential temperature source S'_θ, which represents convective heating. As a simple model of S'_θ for a tilted wave, consider a two-dimensional (x–z) setup and a heat source with two phase-lagged baroclinic modes: $S'_\theta = k\cos(kx - \omega t)\sqrt{2}\sin(z) + \alpha k\cos[k(x+x_0) - \omega t]\sqrt{2}\sin(2z)$. Two key parameters here are α, the strength of the second baroclinic heating, and x_0, the lag between the heating in the two vertical modes. The vertical velocity is then given by WTG balance, $w' = S'_\theta$, and the zonal velocity is given by the continuity equation, $u'_x + w'_z = 0$:

$$u'(x,z,t) = -\sin(kx - \omega t)\sqrt{2}\cos(z) - 2\alpha\sin[k(x+x_0) - \omega t]\sqrt{2}\cos(2z), \quad \text{and} \tag{18}$$

$$w'(x,z,t) = k\cos(kx - \omega t)\sqrt{2}\sin(z) + \alpha k\cos[k(x+x_0) - \omega t]\sqrt{2}\sin(2z). \tag{19}$$

Although they will not be needed for the exposition here, the thermodynamic variables in this model are given by the balance equations $p' = \Phi'_s$ and $\theta' = p'_z$, where Φ'_s is the velocity potential for momentum sources.

With this form of u' and w', the eddy flux divergence is

$$\partial_z\langle\overline{w'u'}\rangle = \frac{3\alpha k}{2}\sin(kx_0)[\cos(z) - \cos(3z)]. \tag{20}$$

Notice that a wave with first and second baroclinic components generates CMT that affects the first and *third* baroclinic modes (MB04; BM05). The third baroclinic mode was not included in earlier work with the multicloud model, and a third baroclinic wave momentum $u'_3(x,t)$ for the fluctuations is still not included here. However, a third baroclinic mode mean flow, $\bar{U}_3(T)$, is included in (14) in the model used here to capture the large-scale effect of CMT, and it will play an important role in the dynamics. Also notice that (20) is nonzero as long as $\alpha \neq 0$ (i.e., there are both first and second baroclinic mode contributions) and $x_0 \neq 0$ (i.e., there is a phase lag between the first and second baroclinic modes). The CCWs in the multicloud model typically have this structure (KM06c; KM08b).

f. Numerical methods

The model used here involves dynamics on two time scales. The waves u' evolve on a fast time scale t as

$$\frac{\partial u'}{\partial t} = f(u', \bar{U}), \tag{21}$$

and the mean flow $\bar{U}$ evolves on a slow time scale $T = \epsilon^2 t$ as

$$\frac{\partial \bar{U}}{\partial T} = g(u', \bar{U}). \tag{22}$$

To solve such a system of equations numerically, two different time steps, Δt and ΔT, are chosen with $\Delta t \ll \Delta T$. Here $\Delta T = 10\Delta t$ is used. First, the waves $u'(x, t_0)$ are stepped forward in time with time step Δt to obtain $u'(x, t_0+\Delta t), u'(x, t_0+2\Delta t)$, etc., while the mean flow $\bar{U}(t_0)$ is held frozen. Because $g(u', \bar{U})$ in (22) involves time and space averages such as $\langle\overline{w'u'}\rangle$, these averages are calculated over the long time interval $\Delta T = 10\Delta t$, after which the mean flow variables $\bar{U}(t_0)$ are updated to $\bar{U}(t_0+\Delta T)$ using (22). Then the cycle is repeated with the waves u' being stepped forward with time step Δt while the mean flow $\bar{U}(t_0+\Delta T)$ is held fixed. See Grabowski (2004) and Majda (2007a) for other examples and references for this technique.

3. Regular intraseasonal oscillations of the mean flow—The simplest scenario

The case shown in this section involves the model in its simplest setup. The results will show an intraseasonal oscillation of the mean variables along with modulations of the CCWs on the same time scale. The CCWs change their propagation direction as the mean variables change, and their CMT (both upscale and downscale) causes the mean variable oscillations. This case uses a trivial climatological base state so that $\bar{U}$ oscillates about the state $\bar{U} = 0$. This case also has a symmetric mean flow evolution between the first and third baroclinic modes, with $\bar{U}_1(T) = -\bar{U}_3(T)$ and $\bar{U}_2(T) = 0$ for all times.

a. Life cycle of the basic oscillation

Figure 1 illustrates one transition of the mean flow $\bar{U}(z,T)$ and CCWs. At time $t = 550$ days, there is a low-level easterly jet and a midlevel shear with $\partial\bar{U}/\partial z > 0$. At this time, the CCWs have not yet developed coherently. By $t = 555$ d, an eastward-propagating CCW has developed. Thus, eastward-propagating CCWs are favored by this mean flow with a low-level easterly jet (and this will be corroborated by the linear stability results shown below). The CCW reaches its peak amplitude at

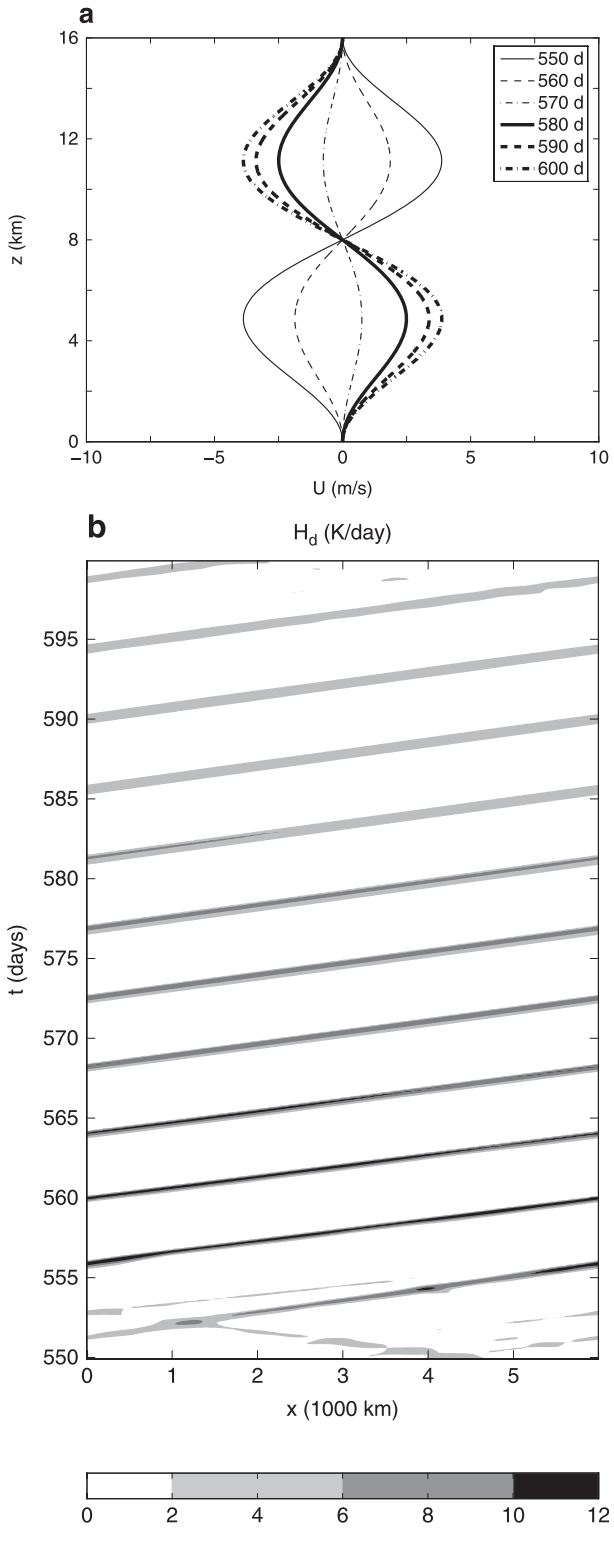

FIG. 1. Regular oscillation with $\bar{U}_1 = -\bar{U}_3$. Evolution of (a) the mean wind $\bar{U}$ and (b) convectively coupled waves through one transition from low-level easterlies to low-level westerlies. The deep convective heating $H_d(x,t)$ is shaded light gray when $H_d > 2$ K day^{-1}, dark gray when $H_d > 6$ K day^{-1}, and black when $H_d > 10$ K day^{-1}.

$t = 555$ to 560 days. At this time, the low-level easterly jet has weakened, and it transitions to a low-level westerly jet by $t = 570$ days. The eastward-propagating CCW tilts from east to west with height. Thus, according to the discussion in section 2e, the CMT of the eastward-propagating CCW first damps the low-level easterly jet and then generates a low-level westerly jet. The amplitude of the low-level westerly jet is then increased in this stage due to upscale CMT from the CCW. A low-level westerly jet, however, is unfavorable for the eastward-propagating CCWs (this will be corroborated by the linear stability results shown below). As long as the CCW propagates eastward, its amplitude continues to weaken, and its CMT continues to strengthen the low-level westerlies, even when its amplitude has weakened. Thus, the CCW weakens until $t = 600$ days, after which a westward-propagating CCW forms, and the next transition repeats in the same fashion.

The multicloud model does not resolve squall lines in detail, yet it is important that the above CCW–mean flow dynamics are broadly consistent with known properties of these mesoscale features. Note that the low-level easterly jet at $t = 555$ to 600 days should also favor westward-propagating squall lines if squall lines were resolved here (Barnes and Sieckman 1984; Dudhia et al. 1987; Nicholls et al. 1988; LeMone et al. 1998; Lucas et al. 2000). In addition, observations and simulations often show CCWs propagating in the opposite direction of the mesoscale convective systems within them (Nakazawa 1988; Grabowski and Moncrieff 2001; Tulich et al. 2007). Thus, the favored propagation direction of the CCWs (eastward) is consistent with what would be expected from observations of squall lines and simulations of multiscale CCWs with the large-scale wind $\bar{U}_3(T)$ determining the sign and strength of the low-level shear.

Figure 2 shows the evolution of the large-scale moisture $\bar{Q}$ and the boundary layer equivalent potential temperature $\bar{\Theta}_{eb}$ presented as deviations from the basic mean sounding, which has been taken as a radiative–convective equilibrium (KM06c; KM08b). These variables oscillate with a period of roughly 50 days as the CCWs intensify and weaken along with the mean flow. Notice that the oscillation amplitude of the fluctuations of $\bar{Q}$ and $\bar{\Theta}_{eb}$ is roughly 0.1 K, which is small compared to the amplitude of q' and θ'_{eb} (roughly 1 K; not shown). All of these values are small compared with the mean thermodynamic base state and reflect the validity of the asymptotic model.

b. Nonlinear propagation dynamics and linear theory

The nonlinear results of Figs. 1–2 can be corroborated by linear stability theory; that is, either eastward- or

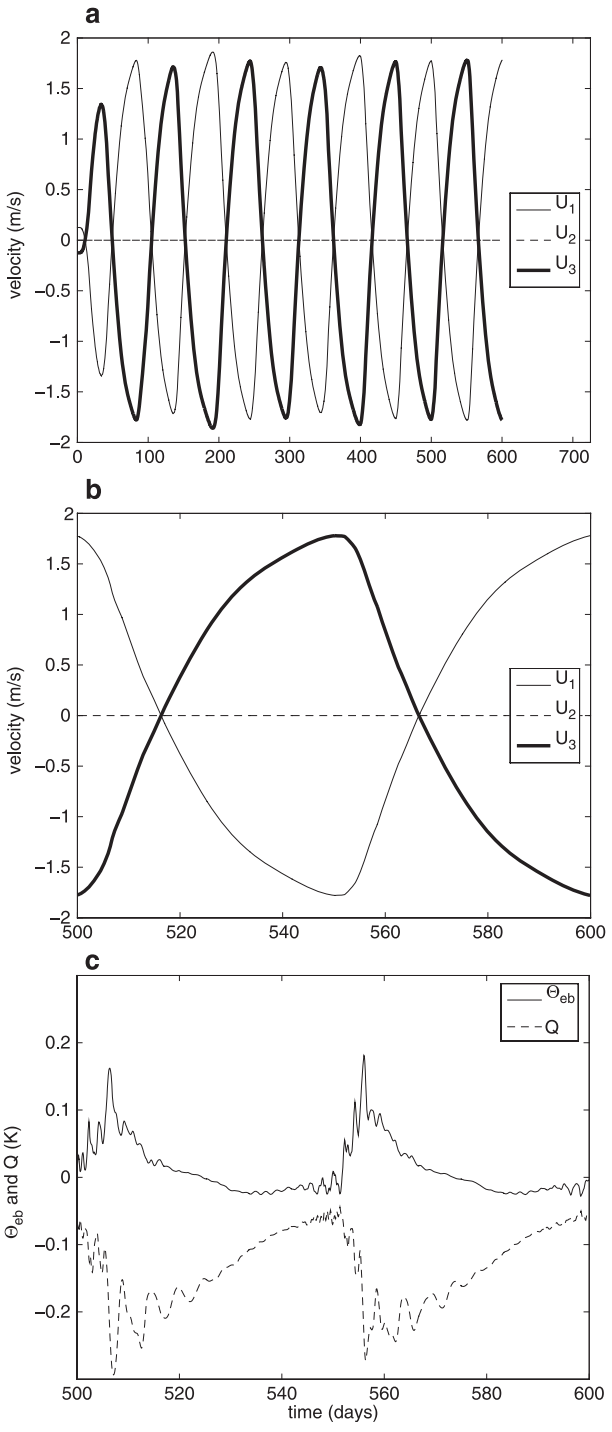

FIG. 2. Regular oscillation with $\bar{U}_1 = -\bar{U}_3$. Evolution of the mean variables: (a) $\bar{U}_1$,$\bar{U}_2$, and $\bar{U}_3$ from $t = 0$ to 600 days, (b) $\bar{U}_1$,$\bar{U}_2$, and $\bar{U}_3$ from 500 to 600 days, and (c) water vapor $\bar{Q}$ and boundary layer equivalent potential temperature $\bar{\Theta}_{eb}$ from 500 to 600 days.

westward-propagating waves are favored depending on the mean flow $\bar{U}$. Linear theory results with a resting background state $\bar{U} = 0$ have been reported for the multicloud model in several earlier papers (Khouider and Majda 2006b; KM06c; KM08b). Here, advection terms have been added to the multicloud model, and results are shown for linear stability theory for the equations in appendix A with a background wind shear. The background shear will be chosen every 10 days from $t = 550$ days to 600 days, which are the times of the snapshots from Fig. 1a.

Linear stability results are shown in Table 2, and results for the case of $t = 550$ days are also shown in Fig. 3. At $t = 550$ days, when there is a low-level easterly jet, the maximum growth rate of the eastward-propagating CCW is more than twice as large as that of the westward-propagating CCW. After $t = 570$ days, when a low-level westerly jet has replaced the low-level easterlies, the westward-propagating CCW has a larger growth rate. This corroborates the nonlinear simulation results shown in Fig. 1.

Figure 4 shows snapshots of the velocity field, including both the wave and mean flow, at times $t = 560$ and 580 days. At $t = 560$ days, there is strong low-level, *front* inflow into the wave, partly due to the low-level easterly jet of the mean flow. At $t = 580$ days, there is a strong *rear*-inflow jet at low levels and weak *front* inflow into the wave; this is partly due to the low-level westerly jet of the mean flow at this time. This change in the inflow into the convective region likely plays a role in the strength of the CCW, and it is clear that changes in the mean flow play a major role in the changes in the inflow.

In Fig. 4a for $t = 560$ days, $\bar{U}_3 > 0$ and there are thus enhanced low-level easterlies in the mean flow, which increase the second baroclinic inflow, wave tilt, and potential congestus preconditioning in this eastward-propagating CCW. On the other hand, in Fig. 4b for $t = 580$ days, $\bar{U}_3 < 0$ and there are thus enhanced low-level westerlies which decrease the second baroclinic inflow, wave tilt, and congestus preconditioning of the eastward-propagating CCW. This intuition is confirmed by the detailed structure of the waves from linear stability analysis reported next. The results above showed that at the most unstable wavelength, the eastward-propagating CCW is favored with the largest growth rate for $\bar{U}_3 > 0$, whereas the westward-propagating CCW is favored for $\bar{U}_3 < 0$. In Fig. 5, bar diagrams from linear theory show the relative strength of wave components of the most unstable eigenvectors (KM06c; KM08b) for $\bar{U}_3 > 0$ at the maximum amplitude for the mean flow. These confirm the above intuition, with approximately 20% larger congestus heating H_c and second baroclinic

TABLE 2. Linear stability theory with the multicloud model with background wind shears from Fig. 1a. Data are shown only for the unstable modes; k_* is the wavenumber (with respect to a 6000-km domain width) of maximum growth rate, γ is the growth rate, and c is the phase speed. Growth rates in columns 4 and 5 correspond to phase speeds in columns 6 and 7, respectively.

Time (days)	$\bar{U}_3$ (m s^{-1})	k_*	γ (k_*) (day^{-1})	c (k_*) (m s^{-1})
550	+1.78	4	0.51 (1.19)	−16.4 (+17.6)
560	+0.86	4	0.68 (1.02)	−16.7 (+17.3)
570	−0.35	4	0.91 (0.78)	−17.1 (+16.9)
580	−1.14	4	1.07 (0.62)	−17.4 (+16.6)
590	−1.55	4	1.15 (0.55)	−17.6 (+16.5)
600	−1.78	4	1.19 (0.51)	−17.6 (+16.4)

wave components u_2 and θ_2 in the favored eastward-propagating CCW compared with the less-favored westward-propagating CCW, whereas the first baroclinic components, u_1 and θ_1, remain unchanged. This decrease in the second baroclinic mode amplitude relative to the first baroclinic mode amplitude amounts to a decrease in the vertical tilts of the CCW, as discussed above in section 2e. The other important quantity for wave tilts is the lag between the first and second baroclinic mode variables, which is the same for the eastward-and westward-propagating waves shown in Figs. 5b,d.

c. Sensitivity studies

To investigate the sensitivity of the oscillation to the domain size, the numerical experiment presented above was carried out using four different periodic domain sizes: 8000, 6000, 4000, and 2000 km. The results already shown used a 6000-km domain width. Table 3 shows how the oscillation changes as the domain size changes. The amplitude of the oscillation is measured by the amplitude of the mean flow jet maximum, which attains its maximum value for the 6000-km domain width. The oscillation time increases as the domain width decreases, ranging from 34 days for 8000 km to 100 days for 2000 km. With a 6000-km domain width, the oscillation time is 53 days, as shown in Figs. 1 and 2 and Table 2. Note from Table 3 that the amplitude of the mean oscillation is not a monotone function of domain width. This reflects the strength of the CCWs, which is a complex function of the mean flow itself, as shown above in section 3b.

In summary, the oscillation time scale is intraseasonal for a range of synoptic-scale domain widths. Why is the time scale intraseasonal? One answer to this question is that the model used here has the same form as an asymptotic model that is derived under the assumption of a separation of time scales; that is, the asymptotic derivation in section 2d predicts self-consistently a separation of time scales between the synoptic-scale waves and the intraseasonal mean variables, and the ansatz in (16) is also consistent with the amplitude of the CCWs in Fig. 4. Note that to check the validity of the asymptotic expansion implied by (16), the fluctuating components need to have a low Froude number as illustrated in Fig. 4, but the magnitude of the large-scale flow $\bar{U}$ just needs to be order one or less in magnitude to retain asymptotic validity. In the present example, the mean flow $\bar{U}$ also has low Froude number throughout the regular oscillation period. Similar remarks apply to the temperature and moisture fluctuations in Fig. 2.

To test the sensitivity of these results to the convective parameterization, we increased the adjustment time for

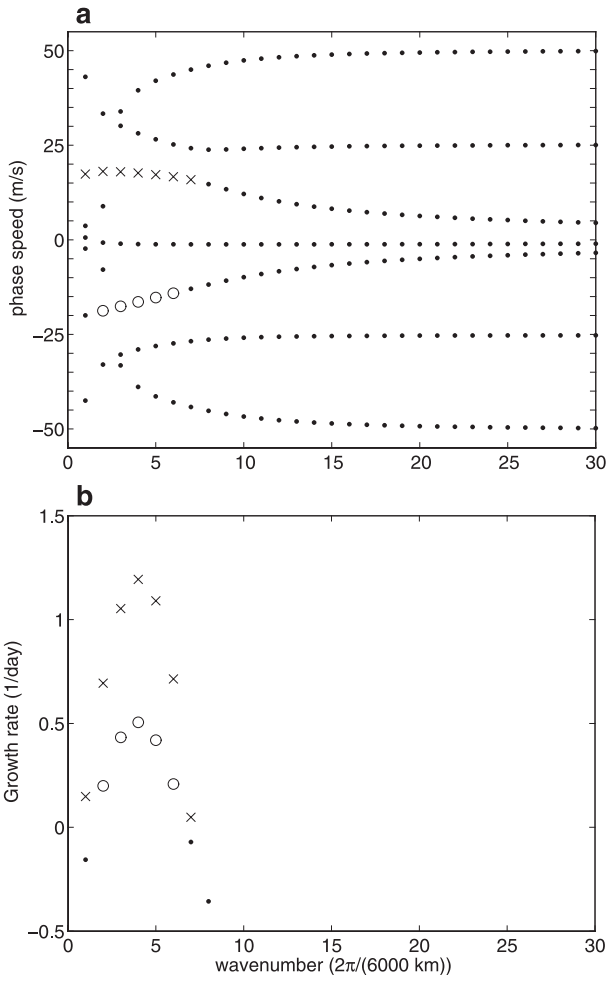

FIG. 3. Linear stability theory with the multicloud model with a background wind shear from Fig. 1a at time t = 550 days: $\bar{U}_1 = -1.78\,\mathrm{m\,s^{-1}}$, $\bar{U}_2 = 0$, and $\bar{U}_3 = +1.78\,\mathrm{m\,s^{-1}}$. (a) Phase speed of linear waves. (b) Growth rates of linear waves. The x axis has units of wavenumber with respect to a 6000-km domain width. Modes with negative growth rates are shown with dots, and two branches of modes with positive growth rates are shown with crosses and open circles.

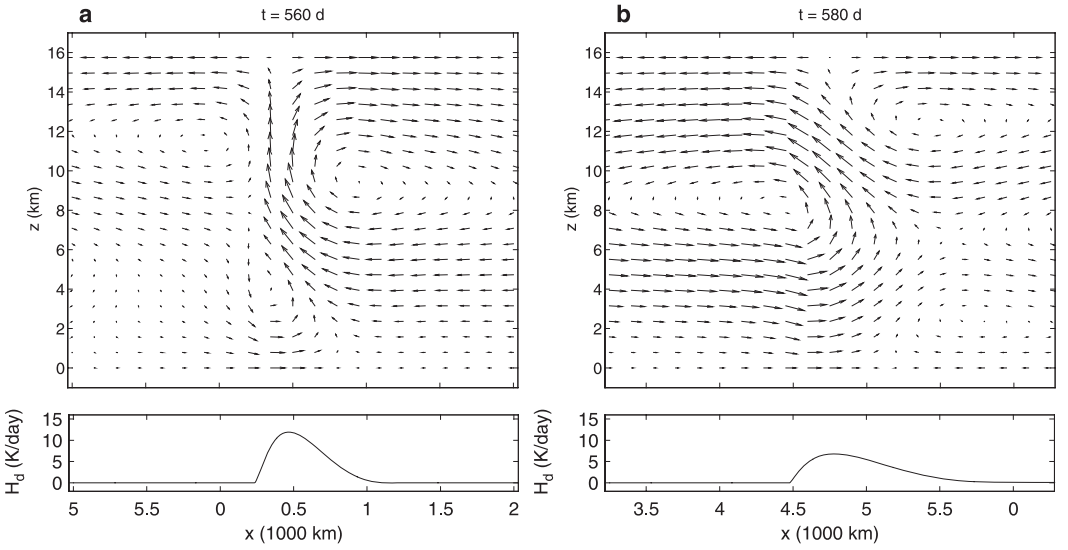

FIG. 4. Snapshots of the velocity field for the eastward-propagating CCW in Fig. 1b at times (a) 560 and (b) 580 days. The maximum velocities in the horizontal and vertical components in (a) are 5.7 m s^{-1} and 7.7 cm s^{-1}, respectively, and in (c) are 4.4 m s^{-1} and 4.3 cm s^{-1}, respectively. Also shown are snapshots of deep convective heating H_d. Note that the x-axis limits are different in (a) and (b).

deep convection from the standard value $\tau_{conv} = 1$ h to $\tau_{conv} = 1.5$ h (see appendix A). For 4000- and 6000-km domains, the oscillation of the mean and character of the CCW dynamics is very similar to the standard case. For a larger domain of 8000 km, the basic oscillation was sustained for the first 200 days of the simulation and then spontaneously decayed when the single propagating CCW changed to two oppositely propagating CCWs. These oppositely propagating CCWs became a standing wave pattern, and, at the same time, the mean wind decayed to zero. With a 10 000-km domain, the standard basic oscillation of the mean wind was restored with a pair of CCWs (essentially wavenumber 2) propagating in the same direction as in the basic oscillation during each organized phase of the waves. There are caveats in utilizing such large-scale domains for the model, as discussed in section 5. All of these facts reflect the sensitive dependence on parameters in turbulent chaotic dynamical systems; the character of the waves in the model depends on the domain size, on τ_{conv}, and on other parameters (KM08b and references therein). The competition between propagating and standing waves described above has also been seen in the multicloud model in a different parameter regime without a mean wind [see the supporting information of Majda et al. (2007)], and it has been described quantitatively for other physical systems through weakly nonlinear perturbation analysis (Bourlioux and Majda 1995). The next section describes other examples with nonzero climatological base states and further interesting dynamical phenomena.

Another parameter that was varied in sensitivity studies is the ratio between the time steps of the fast time scale t and the slow time scale $T = \epsilon^2 t$. All simulations reported here use the standard value $\Delta T = 10\Delta t$ as described in section 2f. The simulation described in Figs. 1–5 was also repeated using $\Delta T = 5\Delta t$, $20\Delta t$, and $50\Delta t$ (not shown), and no differences were seen among the simulations.

4. Irregular intraseasonal oscillations and multiscale waves with a climate base state

In the previous section, the model had a regular oscillation about a resting state $\bar{U} = 0$. If a different initial condition is chosen, an oscillation can develop about a climatological background state with $\bar{U} \neq 0$. Two other climatological regimes are considered in this section. The first regime is similar to the westerly wind burst stage of the MJO, and the second regime is similar to the westerly onset stage of the MJO (Lin and Johnson 1996; Houze et al. 2000; Tung and Yanai 2002a,b; MB04; BM05).

a. Westerly wind burst stage

One case with strong low-level westerlies is shown in Fig. 6. The mean flow oscillates about a climate base state that is mostly first baroclinic (i.e., the cos z term dominates), but CMT causes the maximum low-level winds to shift aloft to $z = 3$ or 4 km, as occurs from $t =$ 1040 to 1070 days. This phase in the cycle of the zonal winds in the simple dynamical model strongly resembles

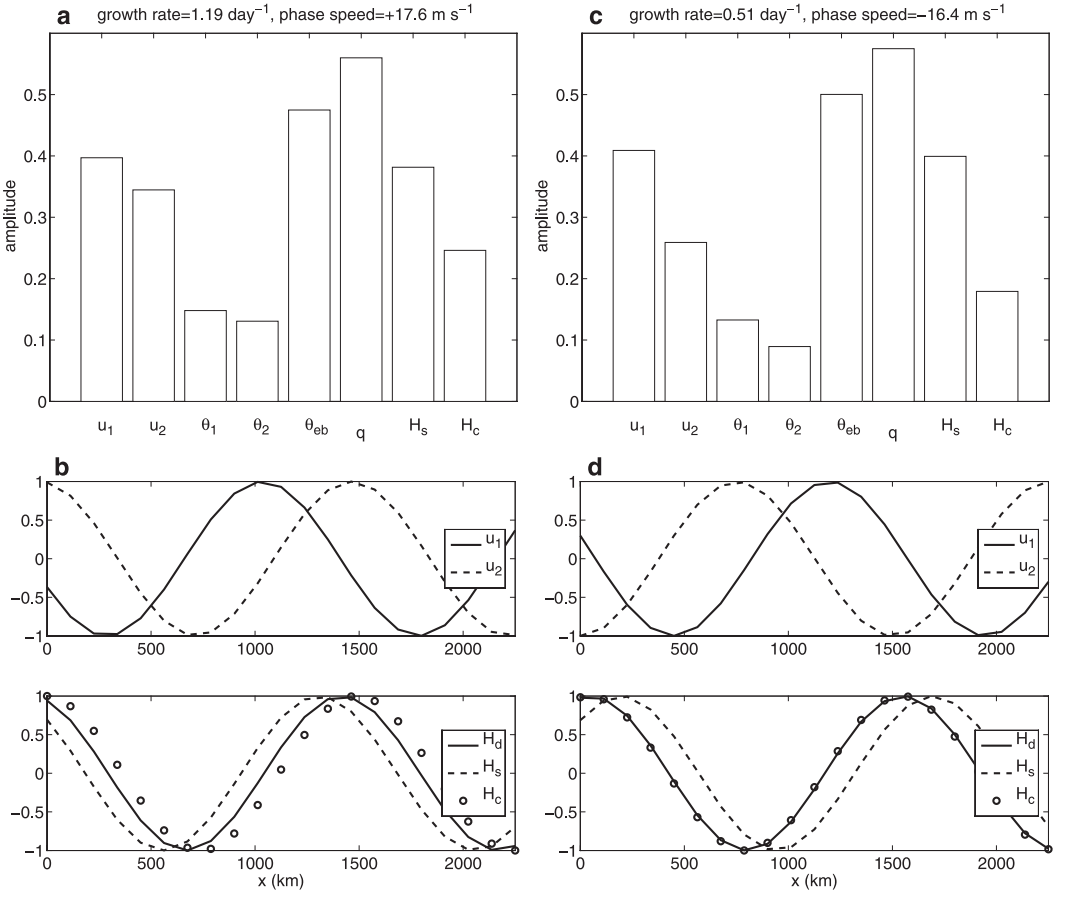

FIG. 5. Linear theory structure of the most unstable (a),(b) eastward- and (c),(d) westward-propagating waves for the case shown in Fig. 3. (a) Absolute value of each component of the unstable eigenvector, which is normalized to have unit magnitude. (b) Phase relationships between different components, with absolute values of all components fixed to 1 to emphasize the phase relationships. The congestus preconditioning H_c and the second baroclinic mode components u_2 and θ_2 are each smaller by more than 20% in the westward-propagating wave [see (a)] compared to the eastward-propagating wave [see (c)]. The phase difference between u_1 and u_2 is almost identical for the eastward- and westward-propagating waves in (b) and (d), respectively.

the one for the zonal winds in the westerly wind burst stage of the MJO from the observational record (Lin and Johnson 1996; Tung and Yanai 2002a,b). First, at time $t = 1040$, the shear is entirely first baroclinic (see Fig. 7) with the maximum of the westerlies at the base of the troposphere as in the westerly onset stage, which is dominated by deep convection. Tung and Yanai (2002a,b) use the diagnostic

TABLE 3. Sensitivity of oscillation to domain width.

Domain width (km)	Oscillation time (days)	Jet max (m s^{-1})	$\bar{U}_3$ max (m s^{-1})
8000	34	2.7	1.25
6000	53	3.9	1.75
4000	63	3.3	1.50
2000	100	2.7	1.25

$$\frac{U(z,T)}{|U|}\frac{\partial U}{\partial t} > 0 \quad (<0) \tag{23}$$

to denote acceleration (deceleration) of the zonal jet where $\partial U/\partial t$ is measured from turbulent transports in the observations. In the westerly wind burst phase of the MJO, they find first a phase of acceleration of the zonal winds in the lower troposphere due to CMT, which is followed by a phase of deceleration of these westerly winds (Tung and Yanai 2002b). This is exactly what happens in the simple model due to CMT as shown in the upper panels of Fig. 6. The zonal winds in the lower troposphere first accelerate between $t = 1040$ to 1070 days when a strong westerly wind burst develops aloft, as in the observations, and then decelerate at the times beyond $t = 1070$ days. Because the first baroclinic shear is large in the present situation with $|U_1| \gg |U_3|$, the

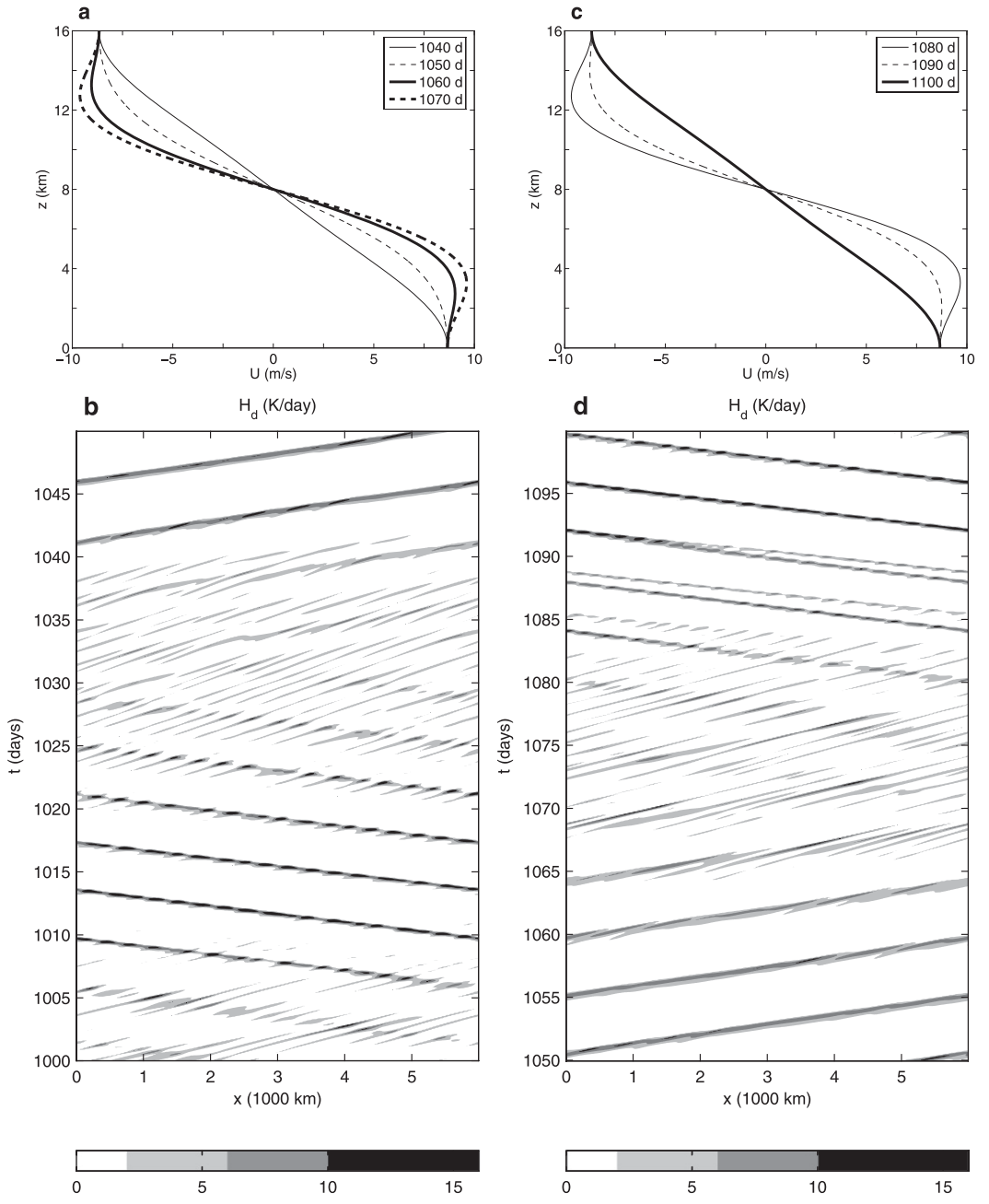

FIG. 6. Irregular oscillations with $\bar{U}_2 = 0$. Plots drawn as described in Fig. 1. (a) Generation of the strong westerly wind burst phase due to upscale CMT; (b) the subsequent decay of this phase due to downscale CMT.

diagnostic of Tung and Yanai (2002a,b) for the low-level westerly winds for 1040 days $\leq t \leq$ 1070 days is essentially $U_1 \partial U_1/\partial t > 0$ (< 0) for acceleration (deceleration) of the low-level westerly winds; the graph of U_1 in Fig. 7b clearly exhibits the same acceleration for 1040 days $\leq t \leq$ 1070 days followed by the deceleration shown in Fig. 6c. These results are in broad agreement with the actual observations of Tung and Yanai (2002b), although this model does not include cumulus friction from unorganized scattered convection, which decelerates the jet more rapidly.

What happens in the simple dynamical model between times t = 1040 and 1070 days is a coherent eastward-propagating CCW (see Fig. 6), which affects the zonal mean flow through CMT as discussed earlier in section 3 and drives the acceleration of the westerly zonal wind.

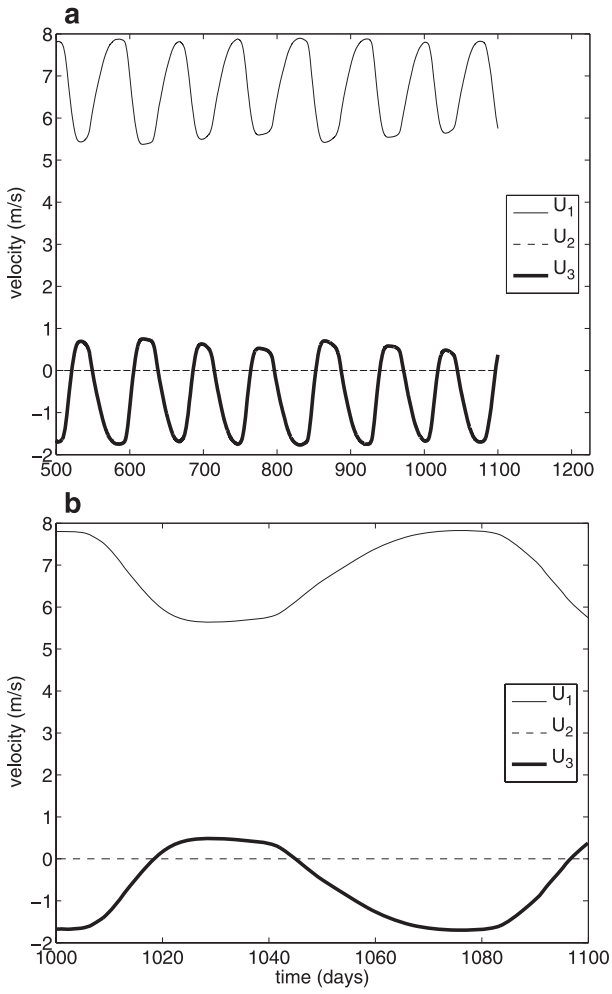

FIG. 7. Irregular oscillations with $\bar{U}_2 = 0$, as in Fig. 6. Evolution of the mean variables $\bar{U}_1, \bar{U}_2$, and $\bar{U}_3$ for times = (a) 500 to 1100 days and (b) 1000 to 1100 days.

Masunaga et al. (2006) has noted the prominent occurrence in observations of eastward-propagating convectively coupled Kelvin waves in the westerly wind burst phase of the MJO. This occurs, for instance, as the CCW propagates eastward from $t = 1040$ to 1070 days. [This is also the same role played by eastward-propagating superclusters in a recent diagnostic multiscale model of the MJO (MB04; BM05).] Note that this analogous behavior occurs in this simple dynamical model even though it is one-dimensional horizontally and without Coriolis effects.

The most striking feature of Fig. 6 is the occurrence of multiscale waves with envelopes propagating westward with smaller-scale convection propagating eastward within the envelope. These multiscale waves appear in the transition phases between instances of coherent CCWs propagating in opposite directions. At these stages, the wave patterns resemble those in the CRM simulations of Grabowski and Moncrieff (2001). The occurrence of both coherent and scattered convection is also reminiscent of the CRM simulations in Grabowski et al. (1996), although their results were on smaller scales and their mean variables were prescribed, not dynamic.

Figure 7 shows the evolution of $\bar{U}$, which indicates how CMT changes with time. The most rapid changes in $\bar{U}$ occur in the presence of intense westward-propagating CCWs, whereas the CMT is nearly zero (i.e., $\bar{U}$ is slowly changing) while the multiscale waves are present. This demonstrates that waves are most effective at generating CMT when they are both coherent and intense.

Figure 8 and Table 4 show linear stability theory that corroborates these results. For the mean flow with the strongest westerlies aloft near $z = 3$–4 km, which occurs around $t = 1000$ and 1070 days, the most unstable waves are westward-propagating with wavelengths of 1200–1500 km. However, there is also a wide band of unstable eastward-propagating waves at smaller scales. This is consistent with the multiscale waves that appear at these times. The smaller-scale band of unstable modes is less pronounced at time $t = 1030$, but the eastward- and westward-propagating waves have similar growth rates. Consistent with this, there are multiscale waves at this time in Fig. 7.

b. *Westerly onset stage*

Figure 9 shows three cases similar to the westerly onset stage of the MJO. The three cases differ in the strength of $\bar{U}_2$, which takes the values 3, 4, and 5 m s^{-1}. Each case has a midlevel easterly jet and westerlies at low levels. The case in Figs. 9a,b uses $\bar{U}_2 = 3$ m s^{-1}, and the mean wind variables $\bar{U}_1$ and $\bar{U}_3$ show an irregular oscillation. The transition times of the mean wind vary widely from roughly 50 to 100 days. The longer, 100-day transitions appear to coincide with waves of wavenumber 2 (not shown). This is consistent with the results above, which showed the strongest CMT coming from intense, coherent CCWs and weaker CMT coming from multiscale CCWs.

Figures 9c–f show the cases with $\bar{U}_2 = 4$ and 5 m s^{-1}. These cases show small-amplitude oscillations about a midlevel jet and decay to a midlevel jet, respectively. This type of behavior is characteristic of a Hopf bifurcation (Verhulst 1990). The waves in these two cases propagate both eastward and westward at the same time (not shown), with slight changes in their amplitudes for the case in Figs. 9c,d.

5. Discussion

The results shown in sections 3 and 4 demonstrate why the multicloud model and the mean wind component

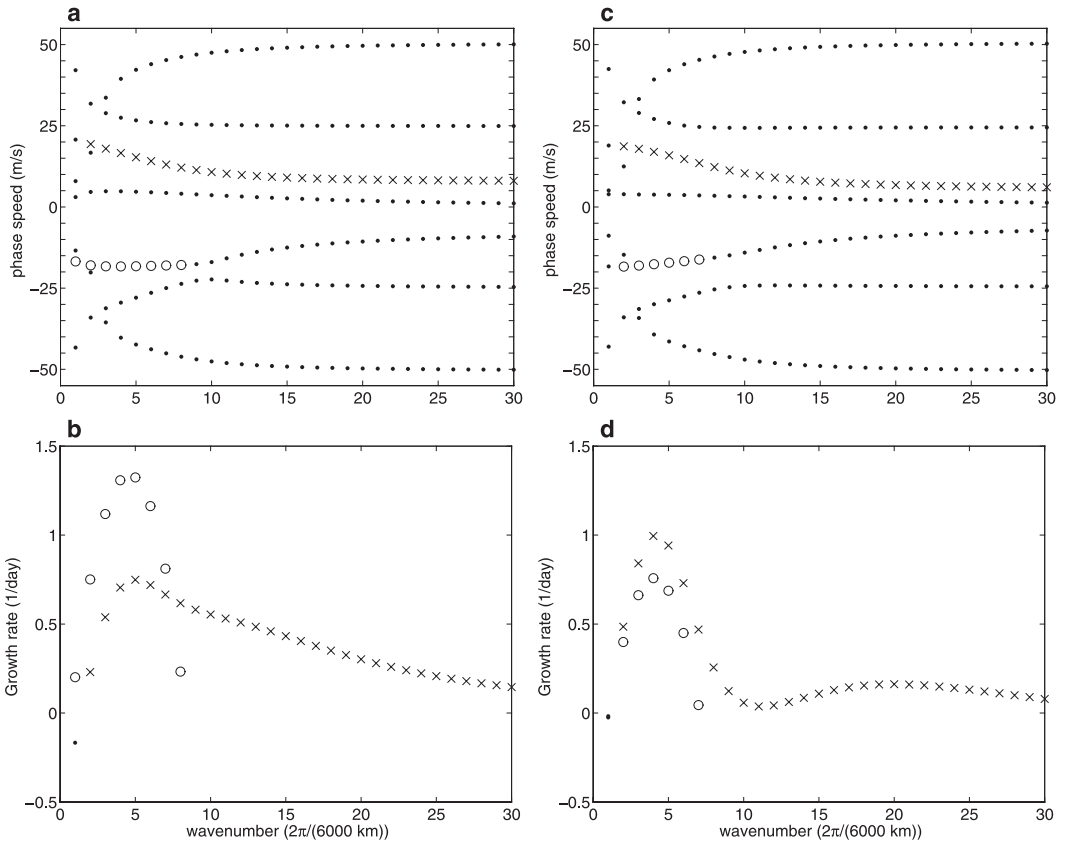

FIG. 8. Linear stability theory with the multicloud model with a background wind shear from Figs. 6 and 7 at times (a),(b) 1005 and (c),(d) 1025 days. Plots drawn as described in Fig. 3.

$\bar{U}_3$ are needed in this convective wave–mean interaction model. One reason is that the multicloud model includes two vertical baroclinic modes, so its CCWs have vertical tilts with nontrivial eddy flux divergence $\partial_z\langle\overline{w'u'}\rangle$; in this way the waves can transport momentum upscale to alter the zonal mean flow in $\bar{U}_1$ and $\bar{U}_3$.

TABLE 4. Linear stability theory with the multicloud model with background wind shears from Figs. 6 and 7. Data are shown only for the unstable modes; k_* is the wavenumber (with respect to a 6000-km domain width) of maximum growth rate, γ is the growth rate, and c is the phase speed. Growth rates in columns 4 and 5 correspond to phase speeds in columns 6 and 7, respectively.

Time (days)	$\bar{U}_3$ (m s^{-1})	k_*	γ (k_*) (day^{-1})	c (k_*) (m s^{-1})
1000	−1.67	5	1.32 (0.75)	−18.2 (+15.3)
1010	−1.27	4	1.21 (0.75)	−18.2 (+16.6)
1020	+0.16	4	0.84 (0.96)	−17.7 (+16.9)
1030	+0.48	4	0.76 (1.00)	−17.6 (+17.0)
1040	+0.37	4	0.78 (0.98)	−17.7 (+16.9)
1050	−0.49	4	1.01 (0.86)	−17.9 (+16.8)
1060	−1.26	4	1.21 (0.76)	−18.2 (+16.6)
1070	−1.65	5	1.30 (0.76)	−18.2 (+15.3)
1080	−1.68	5	1.32 (0.75)	−18.2 (+15.3)

Another reason is that the mean flow component $\bar{U}_3$ affects which waves of the multicloud model are favored—either eastward- or westward-propagating. Furthermore, as demonstrated in section 3, when $\bar{U}_3 > 0$ so that there is an easterly jet shear in the lower troposphere, eastward-propagating CCWs are favored; such an easterly jet shear favors westward-propagating squall line clusters. Thus, the dynamic model for CCW–mean flow interactions on the equatorial synoptic scale is broadly consistent with the fact that, from observations (Nakazawa 1988) and CRM simulations (Grabowski and Moncrieff 2001), embedded squall line clusters propagate opposite to the direction of propagation of CCWs, even though squall lines are not resolved in the present model.

Obtaining the MJO in GCM simulations is a major multiscale challenge, and the results in sections 3 and 4 for the simple dynamical model give insight into the large-scale impact of CMT in the MJO even though the simple model has a single horizontal dimension and no Coriolis effect. As discussed in detail in section 4a for the westerly wind burst scenario, the simultaneous occurrence of eastward-propagating CCWs and first the

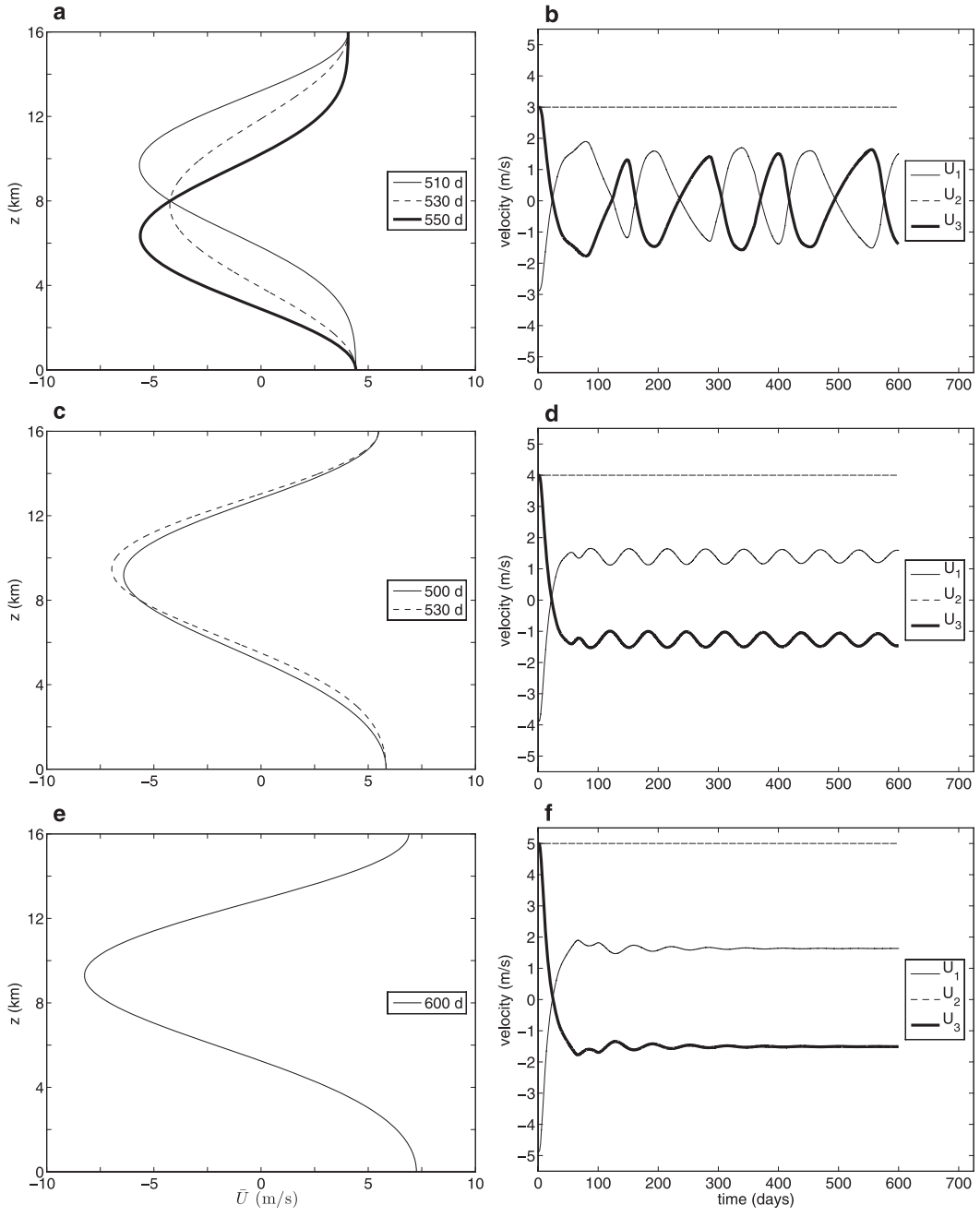

FIG. 9. Irregular oscillations with $\bar{U}_2 \neq 0$. Evolution of the mean wind for varying strength of $\bar{U}_2$: (a),(b) 3, (c),(d) 4, and (e),(f) 5 m s^{-1}.

acceleration followed by the subsequent deceleration of the low-level zonal winds with the strongest westerly winds aloft is analogous to what actually occurs in the observational record during the westerly wind burst phase of the MJO (Tung and Yanai 2002a,b). The results in sections 3 and 4 further support the results of the multiscale diagnostic model of MB04 and BM05, which suggest that upscale CMT from CCWs is crucial for obtaining the full structure of the observed MJO. For instance, in Fig. 6, CMT from eastward-propagating CCWs raises the height of maximum westerlies from the surface to $z = 3$ or 4 km. This is also the role of the superclusters in the multiscale diagnostic model of MB04 and BM05. The results in sections 3 and 4 also suggest that a mean wind varying on intraseasonal time scales could favor or suppress the formation of certain

types of CCWs. It is thus possible that the MJO evolves cooperatively with the CCWs within its envelope, and a successful simulation of the MJO in GCMs may require an accurate representation of CCWs as well (Lin et al. 2006).

The behavior of CMT in the simple dynamical model also has direct contact with the behavior found in the CRM simulations of Grabowski and Moncrieff (2001). These CRM simulations occur on a planetary-scale domain of 20 000 km in a single horizontal dimension without Coriolis effects and show the clear development of a wave train of CCWs moving eastward with embedded westward-propagating squall lines for a time period of 40 days. Figure 16 of that paper demonstrates large synoptic-scale CMT present in these wave trains of CCWs; the simple model developed here captures the effect of CMT of such synoptic-scale CCWs on the zonal winds and their two-way interactions on much longer time scales than these simulations and for a synoptic-scale localized wave rather than a planetary-scale wave packet. On the other hand, Fig. 17 of that paper demonstrates that the planetary-scale CMT averaged over the global 20 000-km domain is much weaker because of the large areas where there is suppressed convection with no wave activity. These differences point toward the need to generalize the expansion in (16) to include wave packets modulated on the planetary scale in (16) to study the local synoptic-scale transfer of CMT (MB04; BM05; Biello and Majda 2009). It is also interesting to note that the damping of Grabowski and Moncrieff (2001) was weaker (with a time scale of 1 day), and CMT was found to play an active role in the formation of CCWs, whereas the damping in the similar simulations of Tulich et al. (2007) was much stronger (with a time scale of 4 h), and CMT was not found to play a role in the CCW dynamics; this is possibly because upscale CMT was not able to overcome the intense prescribed momentum damping. It is possible that a multiscale approach to CMT like the one in sections 2–4 could be useful for simulations of such multiscale waves.

The results in this paper may have implications for other efforts to simulate multiscale waves. Held et al. (1993) use a mesoscale periodic domain of only 640 km. When they allowed CMT to drive the domain-mean flow, their mean flow oscillation had a period of roughly 70 days, and the smaller-scale convection changed its propagation direction as the mean flow changed directions. When they constrained the domain-mean CMT to be zero, the QBO-like oscillation was shut down. The present model cannot be applied directly to analyze these simulations for two reasons. First, the coherent behavior on the smaller scales is due to squall line clusters and, as discussed in the first paragraph of this section, the simple dynamical model does not resolve squall lines and furthermore the synoptic-scale CCWs propagate in the opposite sense, with opposite wave tilts as the squall lines. Second, the mesoscale spatial domain of 640 km is too far below the equatorial synoptic scale of 1500 km to accurately trust the model, and a different nondimensionalization is important. Nevertheless, with these strong caveats, the results in the present paper favor a CMT explanation for this oscillation. The model here demonstrates that a long-time oscillation can result from dynamical CMT interactions between CCWs and a mean wind, in the absence of any stratospheric interactions. However, a different but similar model on mesoscales needs to be developed to confirm that this is also possible for squall lines on mesoscales.

6. Conclusions

A simple model with features of CMT was derived and studied. The model included CCWs and zonally averaged mean variables, and it conceptually was of the form

$$\frac{\partial \bar{U}}{\partial T} + \frac{\partial}{\partial z}\langle \overline{w'u'} \rangle = 0$$
$$\frac{\partial u'}{\partial t} + \bar{U}\frac{\partial u'}{\partial x} + w'\frac{\partial \bar{U}}{\partial z} + \frac{\partial p'}{\partial x} = S'_{u,1}.$$

The convective wave–mean interactions were present in eddy flux divergences and in advection of the CCWs by the mean flow. The convective parameterization was the multicloud model of KM06c and KM08b, which captures realistic CCWs with vertically tilted structures. Another key feature was that momentum damping on synoptic scales was parameterized by a drag term $-u'/\tau_u$, but CMT for the large-scale mean flow was driven by the CMT from the resolved synoptic-scale CCWs and can be either upscale or downscale. A systematic asymptotic derivation of the model was also given, and the intraseasonal time scale of the mean variables appears self-consistently.

The simplest scenario with the model involved regular intraseasonal oscillations of the mean variables and CCWs. Within one transition of the mean flow, the CCWs first transport momentum downscale and then upscale, which reverses the sign of the mean flow. After this mean flow reversal, CCWs propagating in the other direction are favored; that is, the CCWs decay and then reappear propagating in the opposite direction. This mechanism was also corroborated by linear stability theory. The oscillation was shown to be intraseasonal over a range of domain sizes, and the maximum amplitude occurred for a 6000-km domain width.

Other cases with climate base states yielded irregular intraseasonal oscillations. In a case with strong low-level westerlies, the mean flow oscillated about a climate base state that is mostly first baroclinic. At the same time, the CCWs had transitions between states of intense, coherent CCWs and multiscale envelopes of CCWs. It was shown that the intense, coherent CCWs had the strongest CMT. Another case showed oscillations with a midlevel easterly jet and westerlies at low levels. Depending on the strength of the midlevel jet, the dynamics can involve large oscillation amplitudes, small oscillation amplitudes, or decay to a steady mean flow with CCWs propagating both eastward and westward at the same time.

These results were discussed in the context of multiscale wave simulations such as CRM simulations of CCWs and GCM simulations of the MJO. It is suggested that multiscale methods may be needed to deal with the subtle issue of resolved CMT on multiple scales.

Acknowledgments. The research of A. M. is partially supported by Grants NSF DMS–0456713 and ONR N0014–07–1–0750. The authors thank Mitch Moncrieff and two anonymous reviewers for suggestions that improved the presentation of the results in this paper.

APPENDIX A

Multicloud Model with Advection

The multicloud model with advection is the following set of seven equations:

$$\frac{\partial u_1}{\partial t}-\frac{\partial \theta_1}{\partial x}=-\frac{1}{\tau_u}u_1-\frac{1}{2\sqrt{2}}\left[6u_2\frac{\partial u_1}{\partial x}+(3u_1+5\bar{U}_3)\frac{\partial u_2}{\partial x}\right], \tag{A1}$$

$$\frac{\partial u_2}{\partial t}-\frac{\partial \theta_2}{\partial x}=-\frac{1}{\tau_u}u_2-2\sqrt{2}\bar{U}_3\frac{\partial u_1}{\partial x}, \tag{A2}$$

$$\begin{aligned}\frac{\partial \theta_1}{\partial t}-\frac{\partial u_1}{\partial x}&=H_d+\xi_s H_s+\xi_c H_c-R_1\\&\quad-\frac{1}{2\sqrt{2}}\left[-2u_2\frac{\partial \theta_1}{\partial x}+4(u_1-\bar{U}_3)\frac{\partial \theta_2}{\partial x}\right.\\&\quad\left.+8\theta_2\frac{\partial u_1}{\partial x}-(\theta_1-9\Theta_3)\frac{\partial u_2}{\partial x}\right],\end{aligned} \tag{A3}$$

$$\begin{aligned}\frac{\partial \theta_2}{\partial t}-\frac{1}{4}\frac{\partial u_2}{\partial x}&=H_c-H_s-R_2\\&\quad+\frac{1}{2\sqrt{2}}\left[-(u_1-\bar{U}_3)\frac{\partial \theta_1}{\partial x}\right.\\&\quad\left.+(\theta_1-9\Theta_3)\frac{\partial u_1}{\partial x}-8\Theta_4\frac{\partial u_2}{\partial x}\right],\end{aligned} \tag{A4}$$

$$\frac{\partial \theta_{eb}}{\partial t}=\frac{1}{h_b}(E-D)+\frac{1}{\pi}\frac{H_T}{h_b}\left(4\theta_2\frac{\partial u_1}{\partial x}+\theta_1\frac{\partial u_2}{\partial x}\right), \tag{A5}$$

$$\begin{aligned}\frac{\partial q}{\partial t}+\tilde{Q}\frac{\partial}{\partial x}(u_1+\tilde{\lambda}u_2)&=-P+\frac{1}{H_T}D\\&\quad-\frac{\partial}{\partial x}[q(u_1+\tilde{\alpha}u_2)],\quad\text{and}\end{aligned} \tag{A6}$$

$$\frac{\partial H_s}{\partial t}=\frac{1}{\tau_s}(\alpha_s P-H_s)+\left(A_s u_1\frac{\partial H_s}{\partial x}+\frac{1}{2}A_s H_s\frac{\partial u_1}{\partial x}\right). \tag{A7}$$

The variables u_j are the jth baroclinic mode velocity, θ_j are the jth baroclinic mode potential temperature, $\theta_{\rm eb}$ is the boundary layer equivalent potential temperature, and q is the vertically integrated water vapor. The source terms for these equations are

$$H_c=\alpha_c\frac{\Lambda-\Lambda^*}{1-\Lambda^*}Q_c, \tag{A8}$$

$$H_d=\frac{1-\Lambda}{1-\Lambda^*}Q_d, \tag{A9}$$

$$P=\frac{2\sqrt{2}}{\pi}(H_d+\xi_s H_s+\xi_c H_c), \tag{A10}$$

$$\begin{aligned}Q_d=\left\{\bar{Q}+\frac{1}{\tau_{\rm conv}}[a_1\theta_{eb}+a_2 q\right.\\\left.-a_0(\theta_1+\gamma_2\theta_2+\gamma_3\bar{\Theta}_3+\gamma_4\bar{\Theta}_4)]\right\}^+,\end{aligned} \tag{A11}$$

$$Q_c=\left\{\bar{Q}+\frac{1}{\tau_{\rm conv}}[\theta_{eb}-a'_0(\theta_1+\gamma'_2\theta_2+\gamma'_3\bar{\Theta}_3+\gamma'_4\bar{\Theta}_4)]\right\}^+, \tag{A12}$$

$$\Lambda=\begin{cases}\Lambda^*, & \text{for } \theta_{\rm eb}-\theta_{\rm em}<\theta^-,\\ \Lambda^*+(1-\Lambda^*)\dfrac{\theta_{\rm eb}-\theta_{\rm em}-\theta^-}{\theta^+-\theta^-}, & \text{for } \theta^-<\theta_{\rm eb}-\theta_{\rm em}<\theta^+,\\ 1, & \text{for } \theta^+<\theta_{\rm eb}-\theta_{\rm em},\end{cases} \tag{A13}$$

$$\theta_{\rm em}=q+\frac{2\sqrt{2}}{\pi}(\theta_1+\alpha_2\theta_2+\alpha_3\bar{\Theta}_3), \tag{A14}$$

$$R_j=\tfrac{1}{\tau_\theta}\theta_j+Q^0_{R,j},\quad j=1,2, \tag{A15}$$

$$\frac{1}{h_b}E=\frac{1}{\tau_e}(\theta^*_{\rm eb}-\theta_{\rm eb}),\quad\text{and} \tag{A16}$$

$$D=\frac{m_0}{P_D}[P_D+\mu_2(H_s-H_c)]^+(\theta_{\rm eb}-\theta_{\rm em}), \tag{A17}$$

where $^+$ denotes the ramp function $f^+=0$ for $f<0$ and $f^+=f$ for $f>0$. The source terms H_c, H_d, and H_s

represent heating from congestus, deep convective, and stratiform clouds, respectively. Radiative cooling is R_j; evaporation is E; downdrafts are D.

These are the equations of the multicloud model of KM08b, with advection terms added using vertical mode projections as described by Stechmann et al. (2008), and with the following changes. Advection terms have been included with zonally averaged variables $\bar{U}_3$, $\bar{\Theta}_3$, and $\bar{\Theta}_4$, which are associated with third and fourth baroclinic mode vertical structures. Advection terms have also been included in the $\theta_{\rm eb}$ equation; these terms ensure conservation of the model's vertically integrated moist static energy (see KM06c), and they can be thought of as environmental downdrafts. Advection terms have also been added to the H_s equation to represent advection of stratiform clouds.

A few source terms have also been changed from KM08b. The congestus heating H_c is treated diagnostically here by taking the limit $\tau_c \to 0$ in KM08b. Also, the parameters γ_2' in Q_c and γ_2 in Q_d take different values here: $\gamma_2' = 2$ and $\gamma_2 = 0.1$. Using a large value of γ_2' emphasizes the second baroclinic mode and gives Q_c the characteristics of a low-level convective available potential energy (CAPE) closure. This change in γ_2' and the use of diagnostic H_c were also necessary to damp small-scale instabilities that sometimes arise when nonlinear advection is added to the multicloud model. The other changes to the source terms are inclusions of $\bar{\Theta}_3$ and $\bar{\Theta}_4$ in (A11)–(A14) with new parameters $\gamma_3 = 0.3$, $\gamma_4 = 0$, $\gamma_3' = 0.5$, $\gamma_4' = 0.25$, and $\alpha_3 = 0.1$; this is done to include feedbacks from the mean thermodynamic variables on the waves. The two momentum drag sources from KM08b have been combined here into a single term with time scale $\tau_u = 3$ days, and the radiative damping time scale used here is $\tau_\theta = 10$ days. The parameter $\alpha_0 = 2$ here, and the parameter $\tau_{\rm conv}$ takes a value of 1 h here instead of $\tau_{\rm conv} = 2$ h as it was in KM08b. This change in $\tau_{\rm conv}$ reduces the wavelength of the most unstable waves from 4000 to 1500 km, thereby reducing artificial effects of the wave wrapping around the 6000-km periodic domain and interacting with itself. Without a background shear, reducing $\tau_{\rm conv}$ increases the growth rate of the unstable waves (KM06c), and this is useful for strengthening the CCWs on spatial domains with smaller widths like 6000 km. Besides these changes mentioned above, the parameter values used here are all the same as those in the standard case of KM08b.

The linearized multicloud model equations without background shear have been developed in mathematical detail elsewhere (KM06c; KM08b). It is straightforward to linearize the quadratic advection terms at a mean background shear to produce the complete linearized equations that have been used throughout this paper for linear stability analysis.

APPENDIX B

Asymptotic Derivation of the Model

A derivation using multiscale asymptotics is now given for the multiscale wave–mean model in section 2. This derivation will start from the hydrostatic Boussinesq equations:

$$\partial_t u + \partial_x(u^2) + \partial_z(wu) + \partial_x p = S_u, \tag{B1}$$

$$\partial_t \theta + \partial_x(u\theta) + \partial_z(w\theta) + w = S_\theta, \tag{B2}$$

$$\partial_z p = \theta, \tag{B3}$$

$$\partial_x u + \partial_z w = 0. \tag{B4}$$

A two-dimensional setup is used for simplicity here. These equations have been nondimensionalized using the scales shown in Table 1. The space and time scales x and t represent equatorial synoptic scales. The only horizontal spatial variable of the multiscale model is the synoptic-scale variable x, and there are two temporal variables: t represents the synoptic scale and $T = \epsilon^2 t$ represents a longer intraseasonal time scale.

The derivation will involve both space and time averages. The zonal average of a function $f(x, z, t, T)$ is defined as

$$\bar{f}(z,t,T) = \lim_{L\to\infty} \frac{1}{2L} \int_{-L}^{L} f(x,z,t,T)\, dx. \tag{B5}$$

Using this average, any function can be split into a zonal average and fluctuation: $f(x,z,t,T) = \bar{f}(z,t,T) + f'(x,z,t,T)$, where f' is defined as $f - \bar{f}$. The temporal average over the synoptic scales is defined similarly as

$$\langle f \rangle(x,z,T) = \lim_{\tilde{T}\to\infty} \frac{1}{2\tilde{T}} \int_{-\tilde{T}}^{\tilde{T}} f(x,z,t,T)\, dt. \tag{B6}$$

The ansatz for the velocity u includes an $O(1)$ large-scale average $\bar{U}(z,T)$ and an $O(\epsilon)$ fluctuation $\epsilon u'(x, z, t, T)$, with similar expansions for the other variables:

$$u = \bar{U}(z,T) + \epsilon u'(x,z,t,T) + \epsilon^2 u_2 + O(\epsilon^3), \tag{B7}$$

$$\theta = \bar{\Theta}(z,T) + \epsilon\theta'(x,z,t,T) + \epsilon^2\theta_2 + O(\epsilon^3), \tag{B8}$$

$$p = \bar{P}(z,T) + \epsilon p'(x,z,t,T) + \epsilon^2 p_2 + O(\epsilon^3), \quad \text{and} \tag{B9}$$

$$w = \epsilon w'(x,z,t,T) + \epsilon^2 w_2' + O(\epsilon^3). \tag{B10}$$

Notice that $\bar{w} = 0$ because the spatial average of Eq. (B4) yields $\partial_z \bar{w} = 0$.

To obtain the multiscale equations, this ansatz is inserted into (B1)–(B4) and terms are gathered at each order in ϵ. The full temporal derivative of $f(t, \epsilon^2 t)$ must be expanded using the chain rule as $\partial_t f + \epsilon^2 \partial_T f$ to represent the two time scales of the ansatz. When all terms in Eq. (B1) are expanded, the leading-order terms, at $O(\epsilon)$, are

$$\partial_t u' + \partial_x(2\bar{U}u') + \partial_z(w'\bar{U}) + \partial_x p' = S'_{u,1}. \tag{B11}$$

This is an equation for the fluctuations u'. When all terms at $O(\epsilon^2)$ are collected, the result is

$$\partial_t u_2 + \partial_T \bar{U} + \partial_x(u'^2 + 2\bar{U}u_2) + \partial_z\left(\overline{w'u'}\right) + \partial_x p_2 = S_{u,2}. \tag{B12}$$

When a zonal average is applied to this result, the ∂_x terms vanish because $\overline{\partial_x f} = 0$ for any bounded function f by the definition (B5). The terms remaining after the zonal average are

$$\partial_t \bar{u}_2 + \partial_T \bar{U} + \partial_z\left(\overline{w'u'}\right) = 0. \tag{B13}$$

At this point, a key step in the multiscale asymptotic procedure must take place: suppressing secular growth of the higher-order terms (Majda 2003; Majda and Klein 2003; Majda 2007a). The ansatz in (B7)–(B10) assumed that $\epsilon^2 u_2$ has a magnitude of $O(\epsilon^2)$, and this must be maintained or else the asymptotic ordering in (B7)–(B10) would be destroyed. For a time-dependent equation like (B13) of the form $\partial \bar{u}_2/\partial t = F(t)$, secular growth in time is avoided if and only if $\langle F \rangle = 0$. Thus secular growth of $\bar{u}_2$ is avoided if

$$\partial_T \bar{U} = -\partial_z\left\langle \overline{w'u'} \right\rangle. \tag{B14}$$

This is an equation for the large-scale variable $\bar{U}(z, T)$ evolving on the long time scale T. Note that the angle brackets $\langle\ \rangle$ are left off $\bar{U}$ to ease notation.

A similar derivation leads to equations for $\bar{\Theta}$ and θ', and Eqs. (B3) and (B4) are straightforward to separate into orders of ϵ. The result includes a set of equations for the large-scale variables,

$$\partial_T \bar{U} = -\partial_z\left\langle \overline{w'u'} \right\rangle, \tag{B15}$$

$$\partial_T \bar{\Theta} = -\partial_z\left\langle \overline{w'\theta'} \right\rangle + \left\langle \overline{S_{\theta,2}} \right\rangle, \tag{B16}$$

$$\partial_z \bar{P} = \bar{\Theta}, \tag{B17}$$

and a set of equations for the fluctuations,

$$\partial_t u' + \bar{U}\partial_x u' + w'\partial_z \bar{U} + \partial_x p' = S'_{u,1}, \tag{B18}$$

$$\partial_t \theta' + \bar{U}\partial_x u' + w'\partial_z \bar{U} + w' = S'_{\theta,1}, \tag{B19}$$

$$\partial_z p' = \theta', \tag{B20}$$

$$\partial_x u' + \partial_z w' = 0. \tag{B21}$$

This completes the derivation. These equations are then separated into vertical baroclinic modes, and a multicloud convective parameterization is added as shown in section 2.

REFERENCES

Baldwin, M., and Coauthors, 2001: The quasi-biennial oscillation. *Rev. Geophys.,* **39,** 179–229.

Barnes, G., and K. Sieckman, 1984: The environment of fast- and slow-moving tropical mesoscale convective cloud lines. *Mon. Wea. Rev.,* **112,** 1782–1794.

Biello, J. A., and A. J. Majda, 2005: A new multiscale model for the Madden–Julian oscillation. *J. Atmos. Sci.,* **62,** 1694–1721.

——, and ——, 2009: Intraseasonal multiscale moist dynamics of the tropical atmosphere. *Comm. Math. Sci.,* in press.

Bourlioux, A., and A. J. Majda, 1995: Theoretical and numerical structure of unstable detonations. *Philos. Trans. Roy. Soc. London,* **350A,** 29–68.

Dudhia, J., M. Moncrieff, and D. So, 1987: The two-dimensional dynamics of West African squall lines. *Quart. J. Roy. Meteor. Soc.,* **113,** 121–146.

Grabowski, W. W., 2002: Large-scale organization of moist convection in idealized aquaplanet simulations. *Int. J. Numer. Methods Fluids,* **39,** 843–853.

——, 2003: MJO-like coherent structures: Sensitivity simulations using the cloud-resolving convection parameterization (CRCP). *J. Atmos. Sci.,* **60,** 847–864.

——, 2004: An improved framework for superparameterization. *J. Atmos. Sci.,* **61,** 1940–1952.

——, and M. W. Moncrieff, 2001: Large-scale organization of tropical convection in two-dimensional explicit numerical simulations. *Quart. J. Roy. Meteor. Soc.,* **127,** 445–468.

——, X. Wu, and M. W. Moncrieff, 1996: Cloud-resolving modeling of tropical cloud systems during Phase III of GATE. Part I: Two-dimensional experiments. *J. Atmos. Sci.,* **53,** 3684–3709.

Held, I., R. Hemler, and V. Ramaswamy, 1993: Radiative–convective equilibrium with explicit two-dimensional moist convection. *J. Atmos. Sci.,* **50,** 3909–3927.

Hendon, H. H., and M. L. Salby, 1994: The life cycle of the Madden–Julian oscillation. *J. Atmos. Sci.,* **51,** 2225–2237.

Houze, R. A, Jr., S. S. Chen, D. E. Kingsmill, Y. Serra, and S. E. Yuter, 2000: Convection over the Pacific warm pool in relation to the atmospheric Kelvin–Rossby wave. *J. Atmos. Sci.,* **57,** 3058–3089.

Johnson, R. H., T. M. Rickenbach, S. A. Rutledge, P. E. Ciesielski, and W. H. Schubert, 1999: Trimodal characteristics of tropical convection. *J. Climate,* **12,** 2397–2418.

Khouider, B., and A. J. Majda, 2006a: Model multi-cloud parameterizations for convectively coupled waves: Detailed nonlinear wave evolution. *Dyn. Atmos. Oceans,* **42,** 59–80.

——, and ——, 2006b: Multicloud convective parametrizations with crude vertical structure. *Theor. Comput. Fluid Dyn.,* **20,** 351–375.

——, and ——, 2006c: A simple multicloud parameterization for convectively coupled tropical waves. Part I: Linear analysis. *J. Atmos. Sci.,* **63,** 1308–1323.

——, and ——, 2007: A simple multicloud parameterization for convectively coupled tropical waves. Part II: Nonlinear simulations. *J. Atmos. Sci.,* **64,** 381–400.

——, and ——, 2008a: Equatorial convectively coupled waves in a simple multicloud model. *J. Atmos. Sci.,* **65,** 3376–3397.

——, and ——, 2008b: Multicloud models for organized tropical convection: Enhanced congestus heating. *J. Atmos. Sci.,* **65,** 895–914.

Kiladis, G. N., K. H. Straub, and P. T. Haertel, 2005: Zonal and vertical structure of the Madden–Julian oscillation. *J. Atmos. Sci.,* **62,** 2790–2809.

LeMone, M., 1983: Momentum transport by a line of cumulonimbus. *J. Atmos. Sci.,* **40,** 1815–1834.

——, G. Barnes, and E. Zipser, 1984: Momentum flux by lines of cumulonimbus over the tropical oceans. *J. Atmos. Sci.,* **41,** 1914–1932.

——, E. Zipser, and S. Trier, 1998: The role of environmental shear and thermodynamic conditions in determining the structure and evolution of mesoscale convective systems during TOGA COARE. *J. Atmos. Sci.,* **55,** 3493–3518.

Lin, J.-L., and Coauthors, 2006: Tropical intraseasonal variability in 14 IPCC AR4 climate models. Part I: Convective signals. *J. Climate,* **19,** 2665–2690.

Lin, X., and R. H. Johnson, 1996: Kinematic and thermodynamic characteristics of the flow over the western Pacific warm pool during TOGA COARE. *J. Atmos. Sci.,* **53,** 695–715.

Lucas, C., E. Zipser, and B. Ferrier, 2000: Sensitivity of tropical west Pacific oceanic squall lines to tropospheric wind and moisture profiles. *J. Atmos. Sci.,* **57,** 2351–2373.

Madden, R. A., and P. R. Julian, 1972: Description of global-scale circulation cells in the Tropics with a 40–50-day period. *J. Atmos. Sci.,* **29,** 1109–1123.

——, and ——, 1994: Observations of the 40–50-day tropical oscillation—A review. *Mon. Wea. Rev.,* **122,** 814–837.

Majda, A. J., 2003: *Introduction to PDEs and Waves for the Atmosphere and Ocean.* Courant Lecture Notes in Mathematics, Vol. 9, American Mathematical Society, 234 pp.

——, 2007a: Multiscale models with moisture and systematic strategies for superparameterization. *J. Atmos. Sci.,* **64,** 2726–2734.

——, 2007b: New multiscale models and self-similarity in tropical convection. *J. Atmos. Sci.,* **64,** 1393–1404.

——, and R. Klein, 2003: Systematic multiscale models for the tropics. *J. Atmos. Sci.,* **60,** 393–408.

——, and J. A. Biello, 2004: A multiscale model for tropical intraseasonal oscillation. *Proc. Natl. Acad. Sci. USA,* **101,** 4736–4741.

——, and Y. Xing, 2009: New multiscale models on mesoscales and squall lines. *Comm. Math. Sci.,* in press.

——, S. N. Stechmann, and B. Khouider, 2007: Madden–Julian oscillation analog and intraseasonal variability in a multicloud model above the equator. *Proc. Natl. Acad. Sci. USA,* **104,** 9919–9924.

Mapes, B. E., S. Tulich, J. Lin, and P. Zuidema, 2006: The mesoscale convection life cycle: Building block or prototype for large-scale tropical waves? *Dyn. Atmos. Oceans,* **42,** 3–29.

Masunaga, H., T. L'Ecuyer, and C. Kummerow, 2006: The Madden–Julian oscillation recorded in early observations from the Tropical Rainfall Measuring Mission (TRMM). *J. Atmos. Sci.,* **63,** 2777–2794.

Moncrieff, M. W., 1981: A theory of organized steady convection and its transport properties. *Quart. J. Roy. Meteor. Soc.,* **107,** 29–50.

——, 1992: Organized convective systems: Archetypal dynamical models, mass and momentum flux theory, and parametrization. *Quart. J. Roy. Meteor. Soc.,* **118,** 819–850.

——, 2004: Analytic representation of the large-scale organization of tropical convection. *J. Atmos. Sci.,* **61,** 1521–1538.

Nakazawa, T., 1988: Tropical super clusters within intraseasonal variations over the western Pacific. *J. Meteor. Soc. Japan,* **66,** 823–839.

Nicholls, M., R. Johnson, and W. Cotton, 1988: The sensitivity of two-dimensional simulations of tropical squall lines to environmental profiles. *J. Atmos. Sci.,* **45,** 3625–3649.

Roundy, P., and W. Frank, 2004: A climatology of waves in the equatorial region. *J. Atmos. Sci.,* **61,** 2105–2132.

Stechmann, S. N., A. J. Majda, and B. Khouider, 2008: Nonlinear dynamics of hydrostatic internal gravity waves. *Theor. Comp. Fluid Dyn.,* **22,** 407–432.

Tulich, S. N., D. Randall, and B. Mapes, 2007: Vertical-mode and cloud decomposition of large-scale convectively coupled gravity waves in a two-dimensional cloud-resolving model. *J. Atmos. Sci.,* **64,** 1210–1229.

Tung, W.-W., and M. Yanai, 2002a: Convective momentum transport observed during the TOGA COARE IOP. Part I: General features. *J. Atmos. Sci.,* **59,** 1857–1871.

——, and ——, 2002b: Convective momentum transport observed during the TOGA COARE IOP. Part II: Case studies. *J. Atmos. Sci.,* **59,** 2535–2549.

Vallis, G., 2006: *Atmospheric and Oceanic Fluid Dynamics: Fundamentals and Large-Scale Circulation*. Cambridge University Press, 745 pp.

Verhulst, F., 1990: *Nonlinear Differential Equations and Dynamical Systems*. Springer-Verlag, 303 pp.

Wheeler, M., and G. N. Kiladis, 1999: Convectively coupled equatorial waves: Analysis of clouds and temperature in the wavenumber–frequency domain. *J. Atmos. Sci.,* **56,** 374–399.

Wu, X., and M. Yanai, 1994: Effects of vertical wind shear on the cumulus transport of momentum: Observations and parameterization. *J. Atmos. Sci.,* **51,** 1640–1660.

——, and M. Moncrieff, 1996: Collective effects of organized convection and their approximation in general circulation models. *J. Atmos. Sci.,* **53,** 1477–1495.

——, L. Deng, X. Song, and G. Zhang, 2007: Coupling of convective momentum transport with convective heating in global climate simulations. *J. Atmos. Sci.,* **64,** 1334–1349.

Yanai, M., B. Chen, and W.-W. Tung, 2000: The Madden–Julian oscillation observed during the TOGA COARE IOP: Global view. *J. Atmos. Sci.,* **57,** 2374–2396.

Yang, G., B. Hoskins, and J. Slingo, 2007a: Convectively coupled equatorial waves. Part I: Horizontal and vertical structures. *J. Atmos. Sci.,* **64,** 3406–3423.

——, ——, and ——, 2007b: Convectively coupled equatorial waves. Part II: Propagation characteristics. *J. Atmos. Sci.,* **64,** 3424–3437.

——, ——, and ——, 2007c: Convectively coupled equatorial waves. Part III: Synthesis structures and their forcing and evolution. *J. Atmos. Sci.,* **64,** 3438–3451.